https://doi.org/10.5194/egusphere-2026-4141
Preprint. Discussion started: 9 November 2026
© Author(s) 2026. CC BY 4.0 License.

Source Mineralogy and Transport History Shape the Compositional Heterogeneity of Long-Range Transported Saharan Dust

Julian Weng[1], Yufang Hao[1], Benjamin T. Brem[1], Tianqu Cui[1], Sophie Darfeuil[2], Gaëlle Uzu[2], Jean-Luc Jaffrezo[2], Martin Steinbacher[3], Martine Collaud Coen[4], Thaleia Gkraikou[5], Konstantina Oikonomou[5], Jean Sciare[5], Claudia Mohr[1,6], Andre S. H. Prévôt[1], Martin Gysel-Beer[1], Imad El Haddad[1], and Patrik Winiger[1]

[1]PSI Center for Energy and Environmental Sciences, 5232 Villigen PSI, Switzerland
[2]Université Grenoble Alpes, CNRS, INRAE, IRD, Grenoble-INP, IGE, 38000 Grenoble, France
[3]Swiss Federal Laboratories for Materials Science and Technology, Empa, 8600 Dübendorf, Switzerland
[4]Federal Office of Meteorology and Climatology, MeteoSwiss, 1530 Payerne, Switzerland
[5]Climate and Atmosphere Research Center, The Cyprus Institute, Nicosia, 2121, Cyprus
[6]Department of Environmental Systems Science, ETH Zurich, 8092 Zürich, Switzerland

Correspondence: Patrik Winiger (patrik.winiger@psi.ch)

Abstract.

Mineral dust exerts wide-ranging influences on climate, atmospheric chemistry, and ecosystems, yet its compositional heterogeneity remains poorly represented in global impact assessments. Here, we provide observational constraints and process-level understanding of the compositional variability of long-range transported Saharan dust, including inorganic ions, crustal elements, and trace metals, sampled at the High Altitude Research Station Jungfraujoch (3580 m above sea level) during major dust intrusions between 2011 and 2021. Crustal elements dominate PM_{10} (~45 % from Si, Al, Fe, Ca, K, and Mg) and exhibit the strongest enrichment relative to background concentrations (e.g. factor ~60 for Ti). However, compositional variability differs markedly among species, spanning nearly an order of magnitude for Ca, CO_3^{2-}, S, and Pb, but remaining below a factor of two for Fe and Ti. Combining aerosol observations with satellite remote-sensing retrievals and atmospheric reanalysis, we identify dust source regions and transport history as first-order controls on Saharan dust composition far from source. Soil mineralogy leaves persistent signatures that remain detectable after transcontinental transport, including variations in sedimentary carbonate and clay minerals governing Ca, CO_3^{2-}, and alkali metal fractions. Superimposed, atmospheric processing modifies dust composition through interactions with anthropogenic pollution and size-selective transport, leading to sulfate and heavy-metal accumulation, enhanced crustal-element solubility, and depletion of coarse-mode species like rare earth elements through gravitational settling. These findings demonstrate that mineral dust is not a passive tracer but a compositionally evolving vector linking desert emissions with climate, atmospheric chemistry, and biogeochemical cycling on a global scale.

1 Introduction

Mineral dust is the dominant aerosol by mass in the atmosphere, with a global burden of 22 to 29 Tg, of which northern African sources alone contribute nearly half (11 to 15 Tg) (Kok et al., 2021). Dust emissions have likely doubled since pre-industrial

https://doi.org/10.5194/egusphere-2026-4141
Preprint. Discussion started: 9 November 2026
© Author(s) 2026. CC BY 4.0 License.

times (Hooper and Marx, 2018; Kok et al., 2023). While trends have become less clear in recent decades (Moustaka et al., 2026) and future projections are highly uncertain (Kok et al., 2023), global dust emissions could increase further under intensifying aridity, land degradation, and climate-driven desertification (UNCCD, 2022). Once injected into the troposphere, dust persists for days to weeks and is transported over thousands of kilometers across continents and oceans (Creamean et al., 2013; Yu et al., 2021; Harr et al., 2024), exerting influence on the Earth system at a planetary scale.

These impacts are multifaceted and tightly coupled to ecosystem productivity, climate, and atmospheric chemistry. Deposition of mineral dust supplies essential nutrients to remote ecosystems, sustaining primary productivity in nutrient-deficient regions such as the Amazon basin and the Southern Ocean (Swap et al., 1992; Jickells et al., 2005; Schulz et al., 2012; Moore et al., 2013). At the same time, dust perturbs the Earth's radiative balance both directly — through scattering and absorption of solar radiation (Moteki et al., 2017; Kok et al., 2017) — and indirectly via its interactions with clouds. In particular, mineral dust constitutes the dominant source of ice-nucleating particles in the troposphere (Cziczo et al., 2013; Brunner et al., 2021), thereby exerting a disproportionate influence on mixed-phase and cirrus cloud formation.

Crucially, these Earth system interactions are not governed by dust mass alone, but by its physicochemical properties (Kok et al., 2023). Particle size, mineralogical composition, and mixing state determine how dust absorbs radiation, nucleates cloud droplets and ice, and evolves chemically during transport (Green et al., 2020). The direct radiative effect of dust, for example, depends sensitively on the abundance and speciation of the iron-bearing minerals hematite and goethite (Sokolik and Toon, 1999; Di Biagio et al., 2019), as well as on coatings acquired during atmospheric aging (Seinfeld et al., 2004; Bauer et al., 2007). Likewise, the efficiency of heterogeneous ice nucleation is controlled by specific mineral phases, notably feldspars and quartz, while secondary processing can deactivate or enhance active sites (Boose et al., 2016, 2019; Cziczo et al., 2009). Chemical aging further alters hygroscopicity, as insoluble minerals such as calcite are transformed into soluble salts (Vlasenko et al., 2006; Sullivan et al., 2009), thereby modifying cloud condensation nuclei activity, deposition pathways, and atmospheric lifetime (Kok et al., 2023).

An accurate representation of dust composition and aging is therefore essential for quantifying its climatic and biogeochemical impacts. Yet, despite recent advances, a fundamental gap persists in linking the mineralogical properties of source soils to the composition of airborne dust after long-range transport. Earth system and chemical transport models have only recently begun to move beyond the simplifying assumption of uniform dust composition, incorporating mineral-resolved emission schemes (Gómez Maqueo Anaya et al., 2024; Song et al., 2024). These are informed by field measurement based soil databases such as GMINER (Nickovic et al., 2012) or emerging satellite products from missions like NASA's Earth Surface Mineral Dust Source Investigation (EMIT) (Green et al., 2020).

While these developments may improve agreement with observations, critical limitations remain: First, the connection between soil mineralogy and emitted dust composition remains uncertain, owing to sparse and heterogeneous soil datasets and incomplete representation of size-selective emission processes (Gonçalves Ageitos et al., 2023). Second, the evolution of dust composition during transport — through chemical aging, mixing, and removal — is poorly constrained, limiting our ability to retrace the processing history of observed plumes (Gaston, 2020; Kok et al., 2023). Third, observational datasets capable of

https://doi.org/10.5194/egusphere-2026-4141
Preprint. Discussion started: 9 November 2026
© Author(s) 2026. CC BY 4.0 License.

linking source, transport, and composition in a consistent framework are scarce, particularly for long-range transported dust far from source regions (Gómez Maqueo Anaya et al., 2024; Ratcliffe et al., 2024).

Here, we address these challenges by combining source attribution, transport analysis, and detailed chemical characterization of Saharan dust observed at the High Altitude Research Station Jungfraujoch (JFJ, 3580 m above sea level) in the Swiss Alps. This unique site samples the free troposphere (FT) under conditions representative of long-range aerosol transport (Collaud Coen et al., 2026) while offering minimal regional contamination (Bukowiecki et al., 2016). We analyze the most intense Saharan dust events over more than one decade (2011–2021), leveraging satellite observations and atmospheric reanalysis to constrain source regions, transport pathways, and transit times. By integrating bulk chemical measurements with mass spectrometric analysis into a comprehensive dust mass reconstruction, we directly relate observed compositional variability to both source soil mineralogy and atmospheric transport history. In doing so, we provide a quantitative framework linking emission, transformation, and long-range evolution of mineral dust.

2 Experimental

2.1 Measurement site description

The High Altitude Research Station Jungfraujoch (JFJ, 3580 m above sea level, 46°32′ N 7°59′ E) is located on the ridge between the two alpine summits Jungfrau (4158 m) and Mönch (4110 m) in the Swiss Alps. Owing to its high elevation, the JFJ is situated at a large distance from major pollution sources. It was categorized as *mostly remote* (Henne et al., 2010) and is considered to be one of the monitoring stations with lowest planetary boundary layer (PBL) influence in Europe. Especially in winter, it is located predominantly in the FT (Herrmann et al., 2015). Throughout the last three decades, the JFJ has served as location to investigate transported Saharan dust aerosol, e.g. its deposition, hygroscopic growth, optical properties, cloud condensation nuclei (CCN) and ice-nucleating particle (INP) activity (Schwikowski et al., 1995; Jurányi et al., 2010; Chou et al., 2011; Brunner et al., 2021; Collaud Coen et al., 2026). In the absence of long-range transport events (Saharan dust, wildfire smoke (Masoom et al., 2025), volcanic plumes (Bukowiecki et al., 2011)), the variability of aerosol observations at the JFJ is largely driven by regional PBL intrusions (PBLi) (Baltensperger et al., 1997; Collaud Coen et al., 2011).

2.2 Aerosol sampling, dust event detection and sample selection

Daily PM_{10} aerosol High Volume (HiVol) filters (Pallflex XP56 Tissuquartz 2500QAT-UP, Cytiva, USA) were sampled at the JFJ by the *Swiss National Air Pollution Monitoring Network* (NABEL) using a HiVol sampler (DHA-80, Digitel, Switzerland) (Hueglin et al., 2024). For each 24 h sample, an air volume of 1075 m^3 (actual volume) was filtered. Filters were conditioned at 20 °C and 50 % relative humidity for 96 h prior to gravimetric mass determination and subsequently stored at -23 °C until analysis. Fieldblank filters were collected in an identical way (including the transport to the JFJ) except for exposure to filtration. From HiVol filters, gravimetric PM_{10} was determined by weighing before and after sample collection with a high precision analytical balance with antistatic-kit (XP205, Mettler Toledo, USA).

https://doi.org/10.5194/egusphere-2026-4141
Preprint. Discussion started: 9 November 2026
© Author(s) 2026. CC BY 4.0 License.

Saharan dust events at the JFJ were detected by online optical aerosol measurements, applying a method based on the Ångström exponent of the single scattering albedo (SSA) (Collaud Coen et al., 2004, 2026) (Sect. S1). For all detected events within the period of 2011 to 2021 (at least 12 h of continuous positive detection), daily gravimetric PM_{10} was used to select the 47 sampling days with the highest dust loadings (cf. orange markers in Fig. 2a and dates listed in Table S1). As some of the 47 daily samples are from consecutive days of a single Saharan dust plume arriving at the JFJ, the number of distinct plumes covered in this study is 27.

Although selecting events based on the highest local PM_{10} concentrations may introduce a bias toward more intense dust plumes, we consider this selection essential for establishing process-level understanding. First, high dust loadings ensure a clear separation from local background concentrations, enabling a robust characterization of the chemical composition of long-range transported Saharan dust. Second, the reconstruction of plume origin and transport characteristics is substantially facilitated for pronounced dust events, thereby reducing uncertainties in the obtainment of corresponding parameters (Sect. 2.5). Third, the dust loadings observed locally at the JFJ are strongly influenced by the plume's transport altitude and interactions with the complex Alpine orography. Consequently, also long-range transported dust events showing lower concentrations at the station may nevertheless share similar large-scale characteristics (such as loading and spatial extension) with the events selected here. Therefore, while this event selection is not intended to provide a comprehensive climatological representation of Saharan dust sources and transport to the JFJ, it captures a diverse set of well-defined dust plumes, ideal for process-oriented analyses.

The dust samples — denoted *Dust* hereafter — were chemically analyzed along with a reference set of samples representing background conditions at the JFJ — denoted *Non-Dust* hereafter. For the different chemical analysis methods, *Non-Dust* filters were either pooled to composite samples of four at an interval of four days each for the years 2011 to 2021 ($n = 249$, named composite *Non-Dust*), or analyzed individually on every fourth day from March 2019 to May 2020 ($n = 112$, named daily resolution *Non-Dust*). A schematic of the sample selection strategy is provided in Fig. S1. The *Non-Dust* data set was filtered for samples with considerable Saharan dust influence based on titanium (Ti) mass concentrations (Ti filter thresholds and description of the filtering can be found in Sect. S2.3 and Fig. S2). After filtering, 206 composite *Non-Dust* samples (blue markers in Fig. 2a, yellow markers are removed samples) and 104 daily resolution *Non-Dust* samples remained.

2.3 Chemical analysis of filter samples

Dust filter samples and daily resolution *Non-Dust* samples were analyzed for metal and trace element composition by Inductively Coupled Plasma Mass Spectrometry (ICP-MS, iCAP TQ, Thermo Fisher Scientific, USA), following a full mineralization sample preparation protocol (including hydrofluoric acid digestion). Details on sample preparation and instrumentation are provided in Sect. S4.1. Major water-soluble inorganic ions were measured by Ion Chromatography Mass Spectrometry (IC–MS, INTEGRION and ISQ EC, Thermo Fisher Scientific, USA), using filter water extracts of *Dust* and composite *Non-Dust* samples (details in Sect. S4.2). Bulk water-soluble organic carbon (WSOC) was quantified from water extracts of all sample types by a total organic carbon (TOC) analyzer (TOC-L-series, Shimadzu, Japan), after removal of inorganic carbon (carbonates) by acidification with hydrochloric acid and phosphoric acid (details in Sect. S4.3). Organic carbon (OC) and elemental carbon

https://doi.org/10.5194/egusphere-2026-4141
Preprint. Discussion started: 9 November 2026
© Author(s) 2026. CC BY 4.0 License.

(EC) were analyzed by an OC/EC analyzer (Model 5, Sunset Lab, USA), operated using the National Institute for Occupational Safety and Health (NIOSH) 870 protocol (Birch and Cary, 1996), which allows quantification of carbonate (CO_3^{2-}).

2.4 PM_{10} aerosol mass reconstruction of *Dust* samples

For the *Dust* samples, PM_{10} aerosol mass was reconstructed as follows:

- Nitrate and sulfate of *Dust* samples are not fully neutralized by ammonium at the JFJ, unlike for *Non-Dust*-conditions (cf. the plot of nitrate/sufate-based reconstructed ammonium and measured ammonium in Fig. S3). Consequently, besides ammonium sulfate and filter-based ammonium nitrate, the corresponding non-ammonium-sulfate (NAS) and non-ammmonium-nitrate (NAN) mass concentrations were calculated. The calculations are based on measured ammonium which is attributed to regional PBLi and only to minor extent to transport by Saharan dust (details in Sect. S5.1.1, box plots of ammonium, nitrate and sulfate under *Dust* and *Non-Dust* conditions in Fig. S4 and the good correlation of ammonium with the PBLi tracer NO_y/CO in Fig. S5 with $R^2 = 0.61$). NAS and NAN are attributed to be bound to crustal elements, either from mineral occurrence or through atmospheric processing of precursor gases on dust.
- CO_3^{2-} mass concentrations were calculated from the OC4 fraction of the NIOSH OC/EC protocol (Chow et al., 2001), by referencing to OC4/OC ratios of *Dust* samples in comparison to *Non-Dust* samples (details in Sect. S5.1.2). An excellent correlation of the calculated CO_3^{2-} with ICP-MS quantified Ca — the principal binding partner of carbonate in calcite minerals — is found ($R^2 = 0.98$).
- Oxide (O^{2-}) as a binding partner of crustal elements was calculated by a molar valence balance of crustal cations and anions (details in Sect. S5.1.3). For this, neutralization of cations with O^{2-} was assumed after consideration of NAS, NAN, Cl^- and CO_3^{2-}.
- Besides the crustal elements and trace elements from ICP-MS measurements, silicon (Si) was estimated based on aluminum (Al) mass concentrations, assuming a largely uniform Al-Si-ratio of 2.1 (Caquineau et al., 1998) in the Sahara desert (Sect. S5.2).
- WSOA as a proxy of OA (>80 % water solubility of OA at the JFJ (Weng et al., 2026)) was calculated from WSOC applying median OM/OC-ratios obtained from Offline-Aerosol Mass Spectrometer measurements (Weng et al., 2026) of *Non-Dust* filters (Sect. S5.3).

Consequently, PM_{10} of *Dust* samples was reconstructed considering the following species:

$$\begin{aligned} PM_{10}\ (\text{Dust, reconstructed}) = {} & NH_4NO_3\,(\text{filter}) + (NH_4)_2SO_4 + \text{NAN}\ (NO_3^-) + \text{NAS}\ (SO_4^{2-}) \\ & + CO_3^{2-} + Cl^- + O^{2-} + \text{crustal elements (Table S3)} + \text{WSOA} + \text{EC} \end{aligned} \tag{R1}$$

https://doi.org/10.5194/egusphere-2026-4141
Preprint. Discussion started: 9 November 2026
© Author(s) 2026. CC BY 4.0 License.

A very good agreement of PM_{10} (Dust, reconstructed) with bulk gravimetric PM_{10} was achieved (correlation $R^2 = 0.95$, Fig. S8; $median\ mass\ recovery\ ratio = 0.83\ with\ interquartile\ range\ IQR = 0.77\ to\ 0.88$, Fig. S9). The slight underestimation can be attributed primarily to unaccounted mineral crystal water and adsorbed water on the filters (Sect. S5.4).

2.5 Determination of Saharan dust source regions, plume trajectories and transport times

Source regions, plume trajectories and transport times of the analyzed 27 Saharan dust plumes arriving at the JFJ (Fig. 1) were obtained from a compilation of remote sensing satellite observations and a reanalysis model.

The Spinning Enhanced Visible and InfraRed Imager (SEVIRI) (Schmetz et al., 2002) Dust RGB (Red, Green, Blue) of European Space Agency's (ESA) geostationary satellite Meteosat Second Generation (MSG) was used to determine the dominating dust plume emission source regions and emission start times of each plume. Being based on brightness temperature differences of SEVIRI's IR channels, the Dust RGB offers high spatiotemporal resolution ($3\,\mathrm{km} \times 3\,\mathrm{km}$, $15\,\mathrm{min}$). Source areas and times were retraced by the visual 'back-tracking' method introduced by Schepanski et al. (2007, 2012). In comparison to the receptor time windows (i.e. the duration of the Saharan dust events at the JFJ), the emission time windows remained short in length (in the order of one to few hours). Considering the long-range transport of some of the plumes and the limitations of the MSG SEVIRI Dust RGB product — namely its non-quantitative nature and sensitivity to environmental conditions affecting dust detection (Banks et al., 2019) — a combination of additional satellite and reanalysis products were employed. These were essential for reconstructing dust trajectories from the JFJ to their emission regions and thereby linking observed plumes to individual emission events. The Copernicus Atmosphere Monitoring Service (CAMS) European Centre for Medium-Range Weather Forecasts Atmospheric Composition Reanalysis 4 (EAC4) (Inness et al., 2019), a global atmospheric composition forecasting model constrained by assimilated observations, was used to qualitatively track dust plume transport over large spatial scales through dust aerosol optical depth (AOD) at $550\,\mathrm{nm}$. A more quantitative approach was then applied to approximate daily plume position centroids from emission to arrival at the JFJ: Column-integrated AOD from the Moderate Resolution Imaging Spectroradiometer (MODIS) aboard the polar-orbiting Terra and Aqua satellites of NASA. MODIS AOD offers a quantitative measure for mass loadings of (visible and near-IR) light absorbing atmospheric aerosols, including dust (Sayer et al., 2019). Here, level 3 retrieval products MOD08_D3 (Platnick et al., 2015a) and MYD08_D3 (Platnick et al., 2015b) were used, being available once per day (per each of the two satellites) at a spatial resolution of approximately $110\,\mathrm{km} \times 110\,\mathrm{km}$.

Data origin and processing steps for the satellite and reanalysis model products are described in Sect. S6.1. A discussion of uncertainties associated with the parameter obtainment and an independent validation by online, size resolved PM measurements at the JFJ is provided in Sect. S6.2. An example case with a visualization of all observational products for an individual dust plume is shown in Fig. S11.

https://doi.org/10.5194/egusphere-2026-4141
Preprint. Discussion started: 9 November 2026
© Author(s) 2026. CC BY 4.0 License.

3 Results and Discussion

3.1 Northern and central Saharan source areas produce distinct transport pathways to the JFJ

The long-range transported Saharan dust plumes investigated in this study originate from a broad range of source regions across the Sahara (Fig. 1a, where each determined source region was allocated based on its location to literature *potential source areas*, PSAs (Scheuvens et al., 2013)). Only 10 of the 27 analyzed events (37 %) are associated with the northern source regions PSA1 (Tunisia and northern Algeria) and PSA2a (foothills of Atlas mountains), which are geographically closest to the JFJ (Fig. 1c-1). These plumes are transported almost exclusively along a direct pathway across the Mediterranean Sea towards the JFJ and are characterized by relatively short transport times between 1-2 days (Fig. 1b).

The majority of the plumes (14 out of 27, 52 %) originate from an area around southern Algeria and northern Mali (PSA3). Two distinct transport pathways were identified for these events. One subset is transported rather directly northward towards the JFJ via the Mediterranean Sea (Fig. 1c-2), resulting in transport times of approximately 2-4 days. In contrast, the second subset is initially advected northwestward, subsequently recirculating over the Atlantic before reaching the JFJ via the Iberian Peninsula and France (Fig. 1c-3). These plumes exhibit substantially longer transport times of 5-10 days.

The remaining 3 plumes originate from more variable source regions located in the western and eastern Sahara (Fig. 1c-4).

3.2 Composition and compositional variability of long-range transported Saharan Dust

Intense Saharan dust events (*Dust* samples) increase daily PM_{10} at the JFJ by one to two orders of magnitude relative to background (*Non-Dust*) concentrations (Fig. 2a). Interferences through regional pollution are therefore negligible when interpreting Saharan dust crustal composition. Within the 11-year reference time series, about 17 % of samples were considerably influenced by Saharan dust (Sect. S2.3) and excluded from the *Non-Dust* sample set (yellow markers in Fig. 2a). This frequency agrees well with previous high-temporal-resolution online measurements reporting 17 % of the year 2020 to be affected by Saharan dust (Brunner et al., 2021).

Under *Dust* conditions, PM_{10} at the JFJ is dominated by Si, Al, Fe, Ca, K and Mg (20 %, 9.5 %, 5.0 %, 4.9 %, 2.3 % and 2.0 %, respectively, cf. Fig. 2b), reflecting the elemental composition of the Earth's crust (Fleischer, 1954). Charge balance is primarily maintained by O^{2-}, with additional contributions from CO_3^{2-}, NAN and NAS. In contrast, secondary components such as WSOA and ammonium sulfate — accounting for almost half of the PM_{10} mass under *Non-Dust* conditions at the JFJ (Weng et al., 2026) — contribute a minor fraction (~6 %) during *Dust* events. Nevertheless, these species may influence dust particle properties via surface coating effects (Sullivan et al., 2009; Möhler et al., 2008; Tobo et al., 2012).

Elemental enrichment relative to *Non-Dust* conditions highlights the dominance of crustal material during *Dust* events. In particular, Ti and Fe serve as robust tracers of Saharan dust, with enrichment ratios of 59 and 28, respectively (Table S5), and highly significant differences between *Dust* and *Non-Dust* samples (Mann–Whitney *U* test p-values *Dust* vs. *Non-Dust* in Table S6: 1.0e-15 for Ti and 8.6e-17 for Fe). Most other crustal elements exhibit enrichment ratios clearly exceeding 10 (e.g., Ca: 19, Li: 39, Rb: 27; Table S5). Complementary metalloids and nonmetals feature moderate enrichment (e.g., P: 11, S: 5.1,

https://doi.org/10.5194/egusphere-2026-4141
Preprint. Discussion started: 9 November 2026
© Author(s) 2026. CC BY 4.0 License.

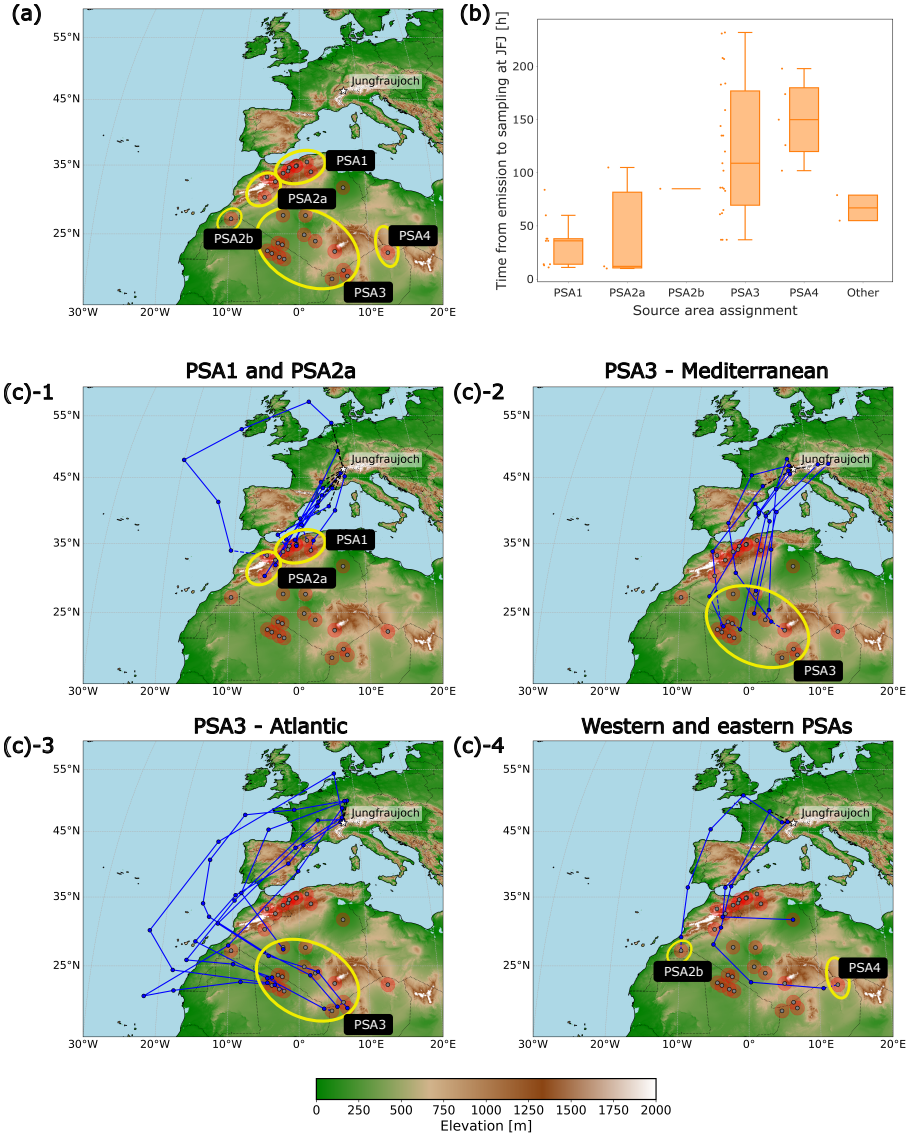


Figure 1. For the investigated Saharan dust plumes, (a) obtained source region centroids (grey with red shaded borders), allocated to major Saharan dust potential source areas (PSA) defined in literature (literature naming provided in the following) (Scheuvens et al., 2013): PSA1 — Tunisia and northern Algeria including the 'zone of chotts', PSA2a — foothills of Atlas mountains , PSA2b — western coastal region , PSA3 — Southern Algeria and northern Mali, PSA4 — Central Libya. (b) Estimated transport times to the JFJ by source area, from emission start to sampling start of the respective filter sample. Event 21-B was not allocated to any PSA and is listed as 'Other'. (c1-4) For different PSAs, obtained transport trajectories of Saharan dust plumes from source regions to the JFJ. Blue points denote approximate daily plume centroid positions after emission.

https://doi.org/10.5194/egusphere-2026-4141
Preprint. Discussion started: 9 November 2026
© Author(s) 2026. CC BY 4.0 License.

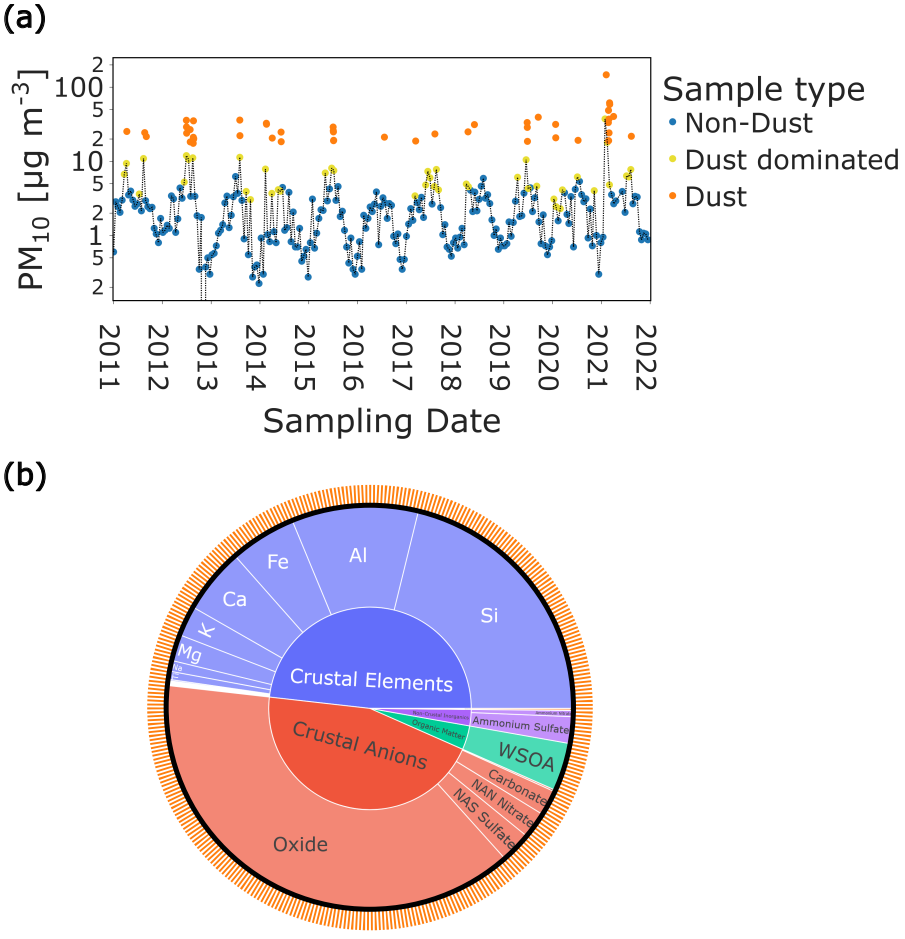


Figure 2. (a) PM_{10} time series from 2011 to 2021 at the JFJ (log_{10} scale). *Non-Dust* composite samples are colored in blue, composite samples flagged as dominated by Saharan dust (Sect. S2.3) in yellow. The separate daily *Dust* samples investigated in this study are shown in orange. (b) Reconstructed aerosol chemical composition under long-range transported Saharan dust conditions at the JFJ. Composition is a median relative composition of the 27 most intense dust plumes between 2011 and 2021. Abbreviations are: WSOA — water-soluble organic carbon, NAN — non-ammonium-nitrate, NAS — non-ammonium-sulfate, Oxide — O^{2-} (in metal oxides).

As: 11, Se: 6.7; Table S5). Heavy metals, which are often associated with anthropogenic sources (Cho et al., 2011; Shafer et al., 2012; Gonzalez et al., 2016), are also enhanced, although to a lesser extent (e.g., Pb: 4.1, Cd: 4.1, Cu: 2.8; Table S5).

Across all 27 distinct plumes analyzed here, long-range transported Saharan dust exhibits considerable chemical heterogeneity (Fig. 3 for elements and Fig. S12 for water-soluble ions). Variability in elemental composition normalized to Al ($c_m/c_m(\mathrm{Al})$), whose mass fraction is relatively homogeneous throughout the Sahara (Scheuvens et al., 2013), reveals distinct groups with substantially higher covariance within groups than between them (Fig. 3a). This pattern reflects geochemical fingerprints arising from shared mineralogical sources or closely related chemical processing (e.g., among chemical analogues).

https://doi.org/10.5194/egusphere-2026-4141
Preprint. Discussion started: 9 November 2026
© Author(s) 2026. CC BY 4.0 License.

Importantly, these groups describe patterns of variability (Fig. 3b) rather than a complete mineralogical association. For example, although Ca occurs in multiple mineral phases, sedimentary carbonate minerals are likely the primary control on its variability in Saharan dust (Scheuvens et al., 2013). The following groups are identified:

- *Alkali metals*: Li, K, Rb, Cs (excluding Na). Rb and Cs closely track K due to isomorphic substitution in K-bearing mineral phases such as feldspars, micas and the mica-like illite (Négrel et al., 2018; Uno et al., 2024). Micas also host Li, and a strong association with Rb and Cs was previously identified (Breiter et al., 2023). A very strong positive correlation between the *Alkali metals* is found (Kendall's $\tau = 0.5$ to 0.9), along with a generally low variability for each component across *Dust* events (Fig. 3b, e.g. IQR of $c_m/c_m(Al)$ for K: 0.21 to 0.27 at a median of 0.24). Strong correlation (Kendall's $\tau = 0.5$ to 0.7) is also observed with the *Sedimentary carbonate minerals* and *Phosphorus group*.

- *Alkaline earth metals*: Be, Sr, Ba. A moderately positive correlation (Kendall's $\tau = 0.4$ to 0.5) and moderately high variability across *Dust* events is observed (e.g. IQR of $c_m/c_m(Al)$ for Ba: 0.0035 to 0.0060 at a median of 0.0047).

- *Sedimentary carbonate minerals*: Mg, Ca, CO_3^{2-}. While also other mineral phases like gypsum ($CaSO_4$) are abundant, variability of Ca (and CO_3^{2-}) is typically associated with the sedimentary mineral calcite ($CaCO_3$) (Scheuvens et al., 2013). Mg closely tracks Ca, reflected in the typical co-occurrence of dolomite ($CaMg(CO_3)_2$) with calcite (Cai et al., 2021). A very strong positive correlation (Kendall's $\tau = 0.7$ to 0.8) and high variability across *Dust* events is observed (e.g. IQR of $c_m/c_m(Al)$ for Ca: 0.39 to 0.72 at a median of 0.53).

- *Heavy metals*: Cr, Cu, Cd, Sn, Pb, Bi. Generally of low mass fraction, these elements are grouped based on their location in the periodic system (d- or p-block), high atomic mass and density. A moderate to strong positive correlation (Kendall's $\tau = 0.2$ to 0.6) and high variability across *Dust* events is found (e.g. IQR of $c_m/c_m(Al)$ for Cr: 0.0018 to 0.0041 at a median of 0.0033). The *Heavy metals* group exhibits a moderate to strong anti-correlation (Kendall's $\tau =$ -0.1 to -0.7) with the *Rare earth metals and actinides*.

- *Rare earth metals and actinides*: Y, La, Ce, Sm, Tb, Ho, Th, U. Of low mass fraction, a strong positive correlation (Kendall's $\tau = 0.4$ to 0.9, with exception of Ce and U) and moderate to low variability across *Dust* events is observed (e.g. IQR of $c_m/c_m(Al)$ for Ce: 0.0010 to 0.0014 at a median of 0.0011).

- *Sulfur group*: S, Se. The chalcogens S and Se have similar chemical properties and interconnected biogeochemical cycles (Feinberg et al., 2020). A very strong positive correlation (Kendall's $\tau = 0.7$) and strong variability across *Dust* events is found (e.g. IQR of $c_m/c_m(Al)$ for S: 0.10 to 0.25 at a median of 0.19). Generally strong correlations (Kendall's $\tau =$ 0.3 to 0.7) are also observed with the *Evaporative minerals* and *Phosphorus group*.

- *Phosphorus group*: P, As, V. P and As are known to act as chemical analogues (Strawn, 2018), and V tends to show similar chemical behavior (all with five valence electrons, tendency for tetrahedral oxyanion XO_4^{3-} formation (Gresser et al., 1986)). A very high positive correlation (Kendall's $\tau = 0.6$ to 0.7) is observed. The variability across *Dust* events is low (e.g. IQR of $c_m/c_m(Al)$ for P: 0.0099 to 0.012 at a median of 0.010).

https://doi.org/10.5194/egusphere-2026-4141
Preprint. Discussion started: 9 November 2026
© Author(s) 2026. CC BY 4.0 License.

– *Evaporative minerals*: B, Na, Br. Based on their high water-solubility and strong correlation to water-soluble ions, these elements were grouped as *Evaporative minerals* (despite the high diversity of evaporative mineral phases, which reaches far beyond these three elements (Warren, 2016b)). Na and Br are typically found in evaporative minerals such as halite (Warren, 2016b; Eggenkamp et al., 2019). Also B occurs in evaporites in the form of borates (Warren, 2016a). Compared to other elements, a very high water solubility is observed for Na and Br (cf. Fig. S12, e.g. median $c_m/c_m(Al)$ for $Na^+/Na = 0.045/0.082 = 0.55$, while for $Mg^{2+}/Mg = 0.015/0.21 = 0.071$). A moderate to good correlation (Kendall's $\tau = 0.3$ to 0.6) is observed between the three elements B, Na and Br, while they exhibit moderate to high variability across *Dust* events (e.g. IQR of $c_m/c_m(Al)$ for Na: 0.072 to 0.11 at a median of 0.082). The *Evaporative minerals* show a generally good to very good correlation (Kendall's $\tau = 0.3$ to 0.8) with water-soluble ions such as K^+, Mg^{2+} and PO_3^{3-} (Fig. S12). Notably, low correlation or even anti-correlation (Kendall's $\tau = 0.1$ to -0.5) is observed between Cl^- and *Evaporative minerals*/water soluble ions. Na is not or only weakly anti-correlated with the *Alkali metals* (Kendall's $\tau =$ -0.1 to -0.3).

A range of other elements, including the relatively abundant Fe, Ti and Mn, show very little variability across *Dust* events (e.g. IQR of $c_m/c_m(Al)$ for Fe: 0.52 to 0.55 at a median of 0.54) and were therefore not assigned to specific geochemical groups. These elements show weak or non-specific correlations with other elements and water-soluble ions (Kendall's τ all within +/–0.5).

Overall, the variability of elemental dust mass fractions presents a highly diverse picture (Fig. 3b). While elements such as Fe and Ti remain relatively constant, others — including Ca, *Heavy metals* and the *Sulfur group* — vary by up to an order of magnitude. Understanding the mechanistic drivers underlying this variability is essential for better constraining the composition and properties of long-range transported Saharan dust.

3.3 Dust source regions and transport history as drivers of compositional heterogeneity

To identify drivers of compositional heterogeneity, a principle component analysis (PCA) was performed on *Dust* samples and interpreted with respect to source regions and transport times derived from satellite remote sensing data. The first two principal components explain more than 60 % of the total variance (Fig. 4). Distinct clustering by source region is evident: samples from the northern Saharan PSA1 and PSA2a cluster at positive PC1 and negative PC2, whereas central Saharan PSA3 and PSA4 occupy the opposite quadrant. This separation is predominately driven by variability in the *Sedimentary carbonate minerals* and *Alkali metals*, as indicated by the PCA loadings (Fig. S13). Mann–Whitney *U* tests of Al-normalized species further confirm significant differences between the dominant source regions PSA1 and PSA3 ($p < 0.005$ for CO_3^{2-}, Mg, Ca, Cs, Rb, K, and Li; Table S7).

In addition to source regions, a second separation is observed with respect to transport time, clearly indicated by the split within the PSA3 samples. Samples with transport times, from emission to receptor, below 120 h show systematically lower PC1 and PC2 scores than those with longer transport durations above 120 h (different green marker symbols in Fig. 4). The *Sulfur group* and *Phosphorus group* contribute most strongly to this separation according to PCA loadings (Fig. S13). Within

https://doi.org/10.5194/egusphere-2026-4141
Preprint. Discussion started: 9 November 2026
© Author(s) 2026. CC BY 4.0 License.

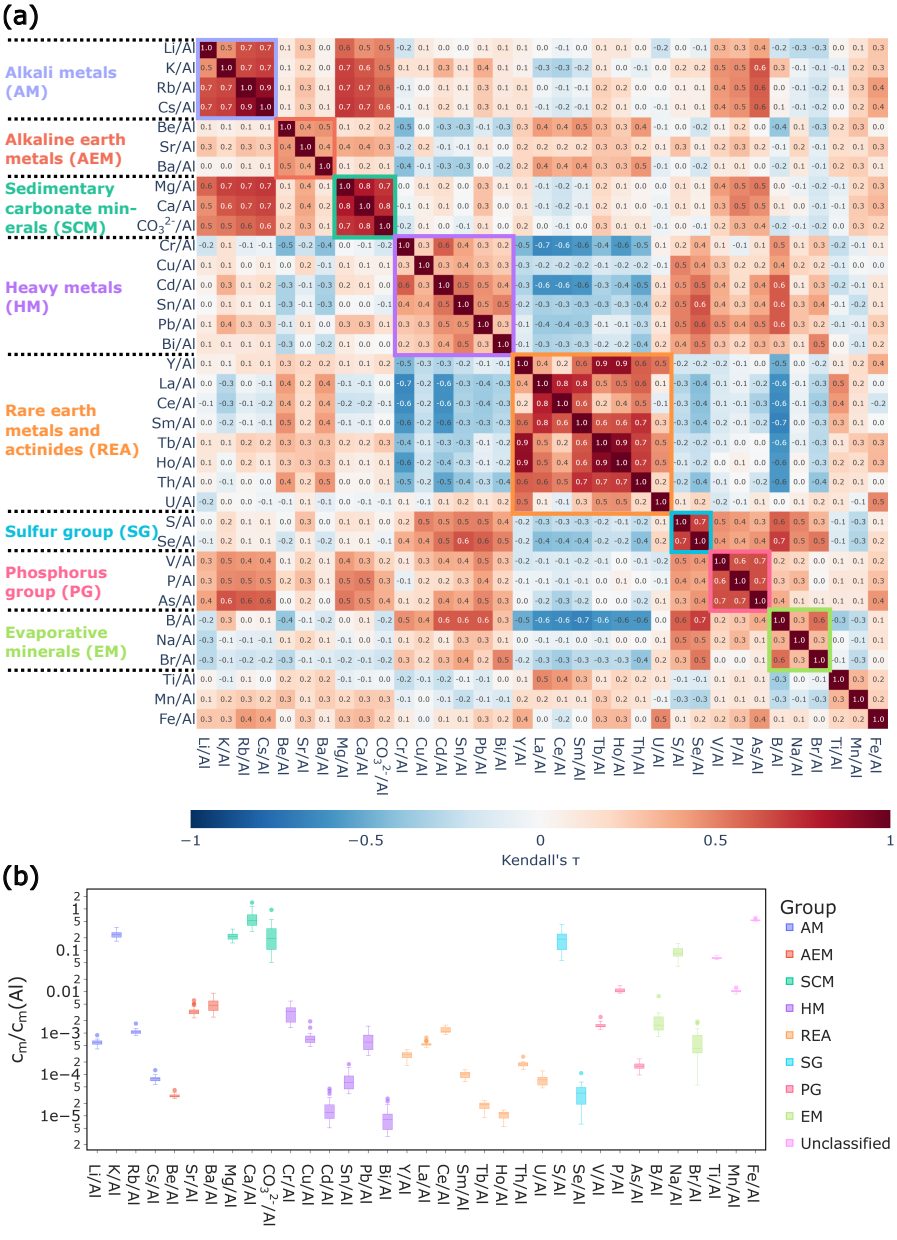


Figure 3. (a) Kendall's τ correlation coefficient matrix of Al-normalized element mass concentrations over all analyzed *Dust* samples. The Al fractional content is relatively homogeneous throughout the Sahara (Caquineau et al., 1998) and therefore applied for normalization of different dust loadings (Scheuvens et al., 2013). Correlation-based geochemical associations were allocated for the species. For simplicity, some elements with low correlations were omitted from the plot. (b) Box plot of Al-normalized mass concentrations of elements for all analyzed *Dust* samples. The species are grouped according to the correlation-based geochemical associations.

https://doi.org/10.5194/egusphere-2026-4141
Preprint. Discussion started: 9 November 2026
© Author(s) 2026. CC BY 4.0 License.

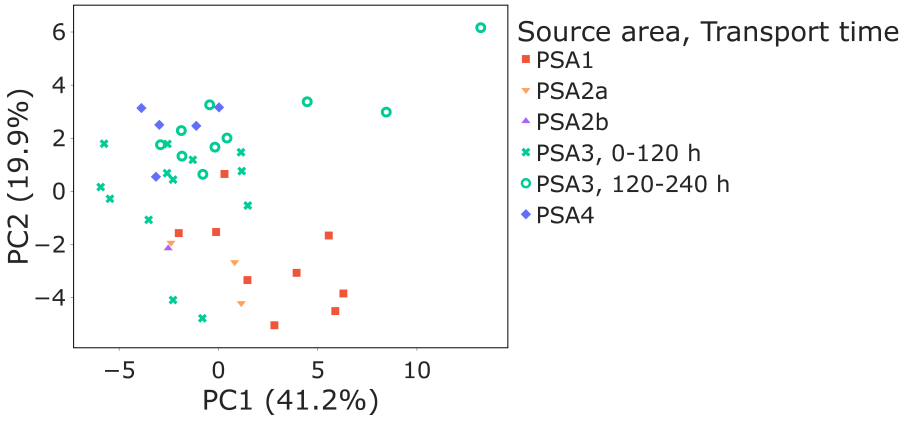


Figure 4. PCA of Al-normalized element and ion mass concentrations of all *Dust* samples with allocated source regions (event 25 was excluded as it strongly clusters as an outlier from all other samples). Marker symbols and color is according to source regions. For PSA3, transport times from emission to sampling start at the JFJ are additionally indicated by different marker symbols (below 120 h: cross; above 120 h: open circle). Standardized data of elements and ions with complete data coverage (above limit of detection) for all displayed *Dust* samples were included in the PCA.

PSA3, Mann–Whitney *U* tests comparing short (<120 h) and long (>120 h) transport times further highlight the role of the *Rare earth elements and actinides* ($p < 0.05$ for Ho, Tb and Y; Table S8).

Together, these results identify both dust source region and transport history, particularly its transport time, as major controls on the compositional heterogeneity of long-range transported Saharan dust.

3.3.1 Dust source regions

Mineralogical variability across the Sahara (Scheuvens et al., 2013; Green et al., 2020; Nickovic et al., 2012) is clearly reflected in the elemental composition of Saharan dust arriving at the JFJ (Fig. 5). The Ca/Al ratio exhibits a pronounced north–south contrast spanning nearly one order of magnitude (Fig. 5a). This pattern is directly related to the high abundance of calcite in northern source regions (PSA1, PSA2a), particularly the Atlas mountain range (Scheuvens et al., 2013), consistent with spatial distributions of topsoil calcite fractions from the *GMINER* database (orange shading in Fig. 5a). Equivalent contrasts are also observed for the other components of the *Sedimentary carbonate minerals* group (CO_3^{2-} and Mg in Fig. S14).

The K/Al ratio also shows a strong north–south gradient (Fig. 5b), which extends to other members of the *Alkali metals* group (Li, Rb, Cs; Fig. S15). This pattern mirrors the large-scale climatic control on weathering intensity and clay mineralogy across the Sahara, particularly the distribution of the clay minerals illite and kaolinite (Caquineau et al., 1998). Kaolinite originates from intense weathering induced destabilization of feldspars and micas, under complete loss of interlayer cations, and predominates in the southern Sahara (reflecting periods of past humid climate conditions). In contrast, the arid northern regions are characterized by illite, a less weathered mica-like clay that retains interlayer K. In a mineralogical context, the K/Al

https://doi.org/10.5194/egusphere-2026-4141
Preprint. Discussion started: 9 November 2026
© Author(s) 2026. CC BY 4.0 License.

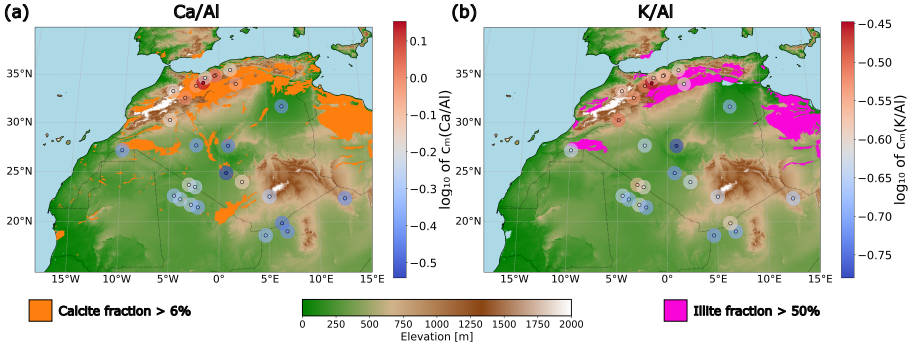


Figure 5. Physical maps showing Saharan dust plume source region centroids colored according to the corresponding log_{10} of Al-normalized mass concentrations of (a) Ca and (b) K measured at the JFJ. Selected mineral contents of dust-productive soils are highlighted according to the *GMINER30* mineralogical database (Nickovic et al., 2012). In (a), regions with clay size ($< 2\,\mu m$) top soil *calcite* content fractions above $6\,\%$ are shaded in orange. In (b), regions with clay size ($< 2\,\mu m$) top soil *illite* content fractions above $50\,\%$ are shaded in pink.

ratio has been applied previously as a proxy for clay mineral weathering (Limmer et al., 2012b, a) and illite abundance (Algeo et al., 2025). The K/Al gradient observed in long-range transported Saharan dust therefore aligns well with the north-south gradient of illite (pink shading in Fig. 5b), reflecting weathering intensity.

In contrast to the *Sedimentary carbonate minerals* and *Alkali metals* groups, the *Heavy metals* and *Sulfur group* show no obvious spatial gradient between source regions (e.g., Pb and Cd in Fig. S16, S and Se in Fig. S17), despite their substantial variability across *Dust* samples (Fig. 3). This suggests that their variability is not primarily source region driven but may instead reflect mixing and secondary processing during transport, including interaction with anthropogenic pollution (Rodríguez et al., 2011).

3.3.2 Dust transport history

Transport history likely exerts a first-order control on dust composition through two coupled mechanisms: (i) Atmospheric uptake and processing, including mixing with anthropogenic pollutants and modification of particle composition through heterogeneous reactions and secondary aerosol formation (Usher et al., 2003; Tang et al., 2017). Although long-range dust transport is generally thought to occur predominantly within the lower FT (Harr et al., 2024), surface-derived pollutants — for example, from the substantial industrial activity across North Africa (Rodríguez et al., 2011) — can be efficiently lofted to these altitudes via the exceptionally deep PBL over the Sahara (Knippertz and Todd, 2012), as well as through orographic mixing along transport pathways over the Atlas Mountains, Pyrenees, and Alps (cf. Figure 1). And (ii) size-selective removal during transport, leading to progressive depletion of more coarse particles and associated species via gravitational settling (cf. $PM_{2.5}/PM_{10}$ in Fig. S10 and van der Does et al. (2016); Ryder et al. (2019)). Element-specific trends with transport time reflect the relative importance of these processes (cf. Kendall's τ in Fig. 6, which includes only samples from a single source region, PSA3; rates of change in Al-normalized element mass concentrations with transport time are also provided in Table S9).

https://doi.org/10.5194/egusphere-2026-4141
Preprint. Discussion started: 9 November 2026
© Author(s) 2026. CC BY 4.0 License.

The *Sulfur group* elements, S and Se, show strong positive correlations with transport time (Kendall's $\tau = 0.44$ for S — Fig. 6c — and 0.52 for Se, both significant at $p<0.005$), indicating net accumulation during long-range transport. This behavior is consistent with ongoing atmospheric processing, particularly heterogeneous oxidation of SO_2 to sulfate on dust surfaces, as previously reported (Huang et al., 2014; Park et al., 2017). The increase in total sulfate concentrations with transport time supports this interpretation (Fig. S18). A similar behavior of Se suggests coupling to sulfur chemistry and/or anthropogenic inputs.

Heavy metals also increase with transport time, showing strong positive correlations (e.g. Kendall's $\tau = 0.50$ for Cd, 0.44 for Pb and 0.46 for Sn, all significant at $p<0.005$). This is consistent with the likely progressive uptake of anthropogenic pollutants during long-range transport (Rodríguez et al., 2011) and aligns with their high inter-sample variability but weak dependence on source regions.

In contrast, the *Rare earth metals and actinides* group exhibits negative correlations with transport time (e.g. Kendall's $\tau =$ -0.52 for Y, -0.49 for Tb and -0.64 for Ho — Fig. 6b —, all significant at $p<0.005$), indicating progressive depletion of their dust fraction. This could be explained by a preferential association of the *Rare earth metals and actinides* group with specific coarse mineral fractions, which are more efficiently removed by gravitational settling.

Other elements, including the *Alkali metals*, *Sedimentary carbonate minerals* and Fe, show no significant dependence on transport time (Kendall's $\tau \approx 0$). For these species, the impacts of chemical processing, pollution uptake and size-selective removal appear to be either weak or compensating on a bulk level. A markedly different picture however is revealed by examining the water-soluble fraction of the crustal elements Ca, Mg, and K. The ratios Ca^{2+}/Ca, Mg^{2+}/Mg, and K^{+}/K increase substantially with transport time (Fig. 7; Kendall's τ = 0.30, 0.45, and 0.48, respectively; all significant at $p<0.05$). This trend points to progressive atmospheric aging, likely driven by processes such as anion exchange with *in-situ* formed nitrate, sulfate or organic acids (as previously observed, for example, for Fe (Johnson and Meskhidze, 2013)). Although these transformations do not alter the bulk elemental fractions, they may significantly modify dust particle properties, including ice nucleation capacity as well as the bioavailability of nutrients.

Overall, the contrasting trends of species demonstrates that transport history integrates both pollution uptake/chemical aging and physical fractionation, with element-specific responses.

4 Atmospheric implications

Despite transport over thousands of kilometers, Saharan dust remains a dominant contributor to aerosol mass in the remote free troposphere, including the JFJ (Collaud Coen et al., 2026). This study shows that long-range transported dust does not converge toward a uniform composition; rather, it retains a resolvable and physically interpretable structure imposed by its origin and subsequently modified during transport. By combining satellite-constrained source attribution with *in-situ* chemical characterization, we demonstrate that source region and transport time act as first-order, and largely separable, controls on dust composition.

https://doi.org/10.5194/egusphere-2026-4141
Preprint. Discussion started: 9 November 2026
© Author(s) 2026. CC BY 4.0 License.

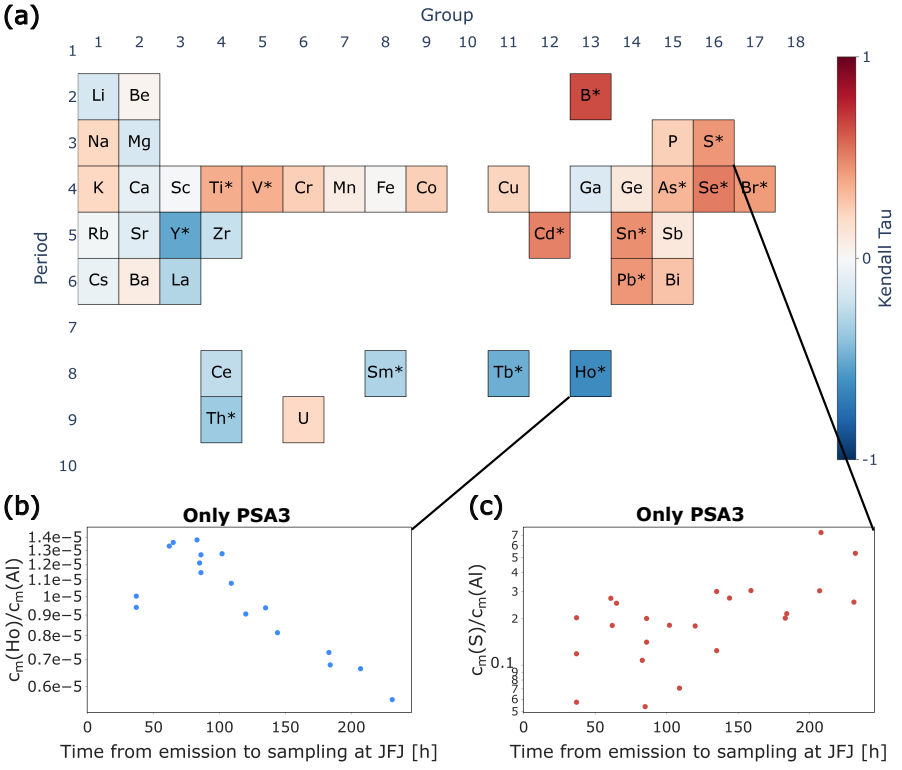


Figure 6. (a) Periodic system colored according to Kendall's τ of Al-normalized mass concentrations of analyzed elements vs dust plume transport time from the emission to sampling start at the JFJ. Only *Dust* samples originating from PSA3 were included. Elements with significant Kendall's τ p-values on a 2σ ($p = 0.05$) criterion are highlighted by an asterisk. For the two elements, (b) holmium and (c) sulfur, the Al-normalized mass concentrations are displayed as a function of dust plume transport time.

Source soil mineralogy imprints a persistent compositional signature on airborne dust, preserved even after multi-day transport across the Mediterranean and Europe. Systematic gradients in sedimentary carbonate- and clay-associated elements directly reflect large-scale mineralogical contrasts across the Sahara, linking emitted particles to their geological origin. This finding establishes that mineralogical heterogeneity at the source propagates into the free troposphere, where it governs key properties relevant for climate (Green et al., 2020). In particular, variability in carbonate content and clay mineralogy directly influences radiative behavior and ice nucleation efficiency (Boose et al., 2016), implying that accurate representation of dust–climate interactions requires explicit consideration of source-resolved mineralogy.

Superimposed on this inherited signature, atmospheric transport exerts a second, equally important control through chemical aging and physical fractionation. Progressive enrichment of sulfate and trace metals with transport time provides clear evidence for sustained interaction with anthropogenic pollution and *in-situ* chemical processing. At the same time, the depletion of rare earth elements and actinides points to size-selective removal, indicating that physical sorting continues to reshape dust composition far from the source. These processes do not simply add secondary species; they fundamentally alter the chemical

https://doi.org/10.5194/egusphere-2026-4141
Preprint. Discussion started: 9 November 2026
© Author(s) 2026. CC BY 4.0 License.

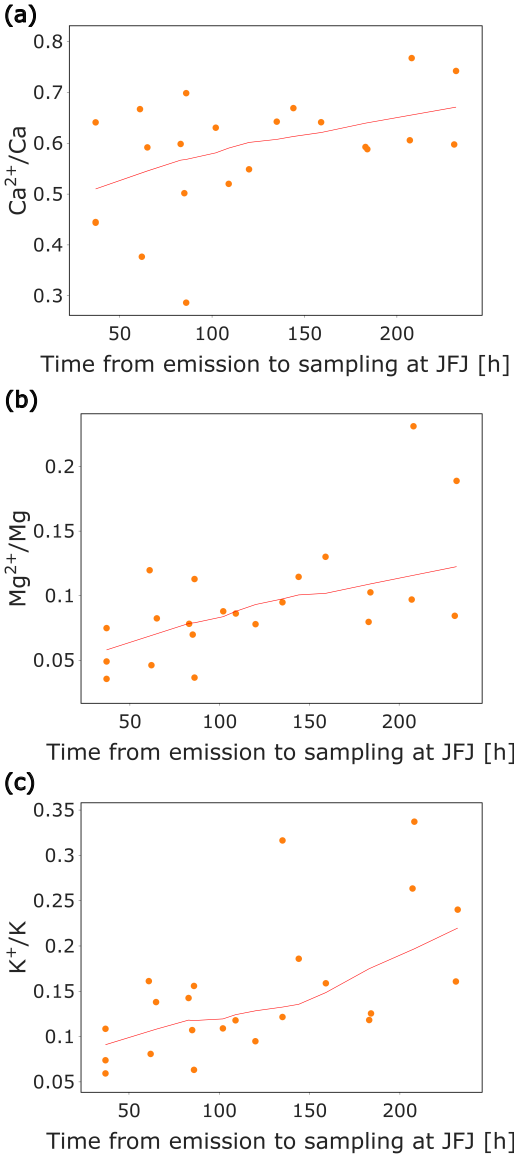


Figure 7. For Saharan dust plumes originating from PSA3, ratios of elemental (ICP-MS) and water-soluble (IC-MS) (a) Ca, (b) Mg and (c) K mass concentrations as a function of dust plume transport time from emission to sampling start at the JFJ. Indicated in red are locally weighted scatterplot smoothing (LOWESS) trend lines. One outlier data point is not displayed in the plots.

and mineralogical state of the particles. The observed increase in solubility of major crustal elements demonstrates that aging transforms dust from a largely inert mineral assemblage into a chemically reactive and bioavailable substrate.

These results have direct implications for the representation of mineral dust in Earth system models. Recent efforts to incorporate mineral-resolved emissions mark a critical step forward (Gómez Maqueo Anaya et al., 2024; Song et al., 2024), but

https://doi.org/10.5194/egusphere-2026-4141
Preprint. Discussion started: 9 November 2026
© Author(s) 2026. CC BY 4.0 License.

our findings show that this is insufficient in isolation. The compositional state of dust arriving in the remote troposphere reflects not only where it originated, but also how it has evolved during transport. Neglecting this evolution obscures key processes controlling radiative forcing, cloud interactions, and nutrient deposition. In particular, the coupling between mineralogy and atmospheric processing — linking, for example, carbonate buffering capacity to heterogeneous chemistry or clay mineralogy to pollutant uptake — remains highly uncertain in current model frameworks (Soussé Villa et al., 2025; Kok et al., 2023).

More broadly, the transformation of dust during transport connects atmospheric chemistry to biogeochemical cycles. Enhanced solubility of iron, phosphorus, and other nutrients increases their bioavailability upon deposition, with consequences for ocean productivity and terrestrial ecosystems (Jickells et al., 2005; Johnson and Meskhidze, 2013). Simultaneously, the accumulation of anthropogenic trace metals introduces a pathway for long-range dispersal of pollutants into otherwise pristine environments. Long-range transported dust thus emerges not as a passive tracer, but as an evolving vector that couples desert emissions to climate, chemistry, and ecosystems on a global scale.

Constraining this evolution requires observational strategies that resolve both sources and processes. High-altitude sites such as the Jungfraujoch, where long-range transport can be sampled with minimal local interference, provide a uniquely powerful platform in this regard. The integration of such *in-situ* observations with satellite-based source attribution offers a pathway toward process-level understanding. Future work should extend this framework to include direct mineralogical measurements, size-resolved composition, and climate-relevant properties such as aerosol absorption, scattering and INP activity. Regarding atmospheric processing and dust–pollution interactions, further investigation is needed into the effects of dust plume spatial extent, loading, composition, and transport altitude, as well as the influence of seasonally and spatially varying vertical mixing strengths of pollutants. Ultimately, only by resolving the coupled effects of source mineralogy and atmospheric processing can we better constrain the role of mineral dust in the Earth system.

Code and data availability. The dataset used to generate all main text and most of the supplementary figures is openly accessible on Zenodo:

- Weng, J., El Haddad, I., Winiger, P., Steinbacher, M., Gkraikou, T., Oikonomou, K., Sciare, J., Ginot, P., Uzu, G., Jaffrezo, J.-L., Darfeuil, S.: Saharan dust plume property and chemical composition data for: Source Mineralogy and Transport History Shape the Compositional Heterogeneity of Long-Range Transported Saharan Dust [data set]. Zenodo. https://doi.org/10.5281/zenodo.20611802, 2026.

The code used for retrieval, processing and visualization of remote sensing satellite and reanalysis model data products is publicly available at GitHub and Zenodo (the exact versions used in this study are archived on Zenodo):

- Weng, J., El Haddad, I., Winiger, P.: Source Mineralogy and Transport History Shape Saharan Dust Compositional Heterogeneity - Remote sensing satellite and reanalysis model data processing and visualization, https://github.com/wengjul/Saharan-dust-remote-sensing-JFJ.git, and archived on Zenodo, https://doi.org/10.5281/zenodo.21032081, 2026.

The code used for data processing and visualization is publicly available at GitHub and Zenodo (the exact versions used in this study are archived on Zenodo):

https://doi.org/10.5194/egusphere-2026-4141
Preprint. Discussion started: 9 November 2026
© Author(s) 2026. CC BY 4.0 License.

– Weng, J., El Haddad, I., Winiger, P.: Source Mineralogy and Transport History Shape Saharan Dust Compositional Heterogeneity - Processing and visualization code, https://github.com/wengjul/Saharan-dust-JFJ.git, and archived on Zenodo, https://doi.org/10.5281/zenodo.21028436, 2026.

Author contributions. According to CRediT taxonomy; **J. W.:** Conceptualization, Data curation, Formal analysis, Investigation, Methodology, Project administration, Software, Validation, Visualization, Writing (original draft preparation), Writing (review and editing). **Y. H.:** Investigation, Methodology, Software, Writing (review and editing). **B.T. B.:** Data curation, Investigation, Writing (review and editing). **T. C.:** Investigation, Methodology, Writing (review and editing). **S. D.:** Investigation, Data curation, Writing (review and editing). **G. U.:** Supervision, Writing (review and editing). **J.-L. J.:** Supervision, Writing (review and editing). **M. S.:** Investigation, Data curation, Writing (review and editing). **M. C.C.:** Data curation, Writing (review and editing). **T. G.:** Investigation, Writing (review and editing). **K. O:** Investigation, Writing (review and editing). **J. S.:** Supervision, Writing (review and editing). **C. M.:** Supervision, Writing (review and editing). **A.S.H. P.:** Supervision, Writing (review and editing). **M. G.-B.:** Data curation, Investigation, Project administration, Writing (review and editing). **I. E.H.:** Conceptualization, Funding acquisition, Investigation, Project administration, Supervision, Writing (review and editing). **P. W.:** Conceptualization, Funding acquisition, Investigation, Project administration, Supervision, Writing (review and editing).

Competing interests. The authors declare that they have no conflict of interest. Part of the funding was provided via a WeMakeIt Science-Booster crowdfunding campaign, including contributions from Digitel AG and Camfil GmbH. The funders had no involvement in the study design, data collection, analysis, interpretation, or manuscript preparation.

Acknowledgements. Mineralogical soil data for visualization was retrieved from the GMINER30 Global Mineral Database of potentially dust productive soils Nickovic et al. (2012), currently available at http://www.seevccc.rs/GMINER30/. (last access: March 6, 2026).

Topography data for plotting of the physical maps was obtained from the NOAA National Centers for Environmental Information ETOPO 2022 global relief model, available at https://doi.org/10.25921/fd45-gt74 (last access: June 19, 2026).

We would like to thank the International Foundation High Altitude Research Stations Jungfraujoch and Gornergrat (HFSJG), 3012 Bern, Switzerland, for enabling us to carry out our experiments at the Jungfraujoch High Altitude Research Station. We also thank the custodians Daniela Bissig and Erich Furrer, Sonja Stöckli and Thomas Furter, Christine and Ruedi Käser, Joan and Martin Fischer, Maria and Urs Otz, Susanne and Felix Seiler for the support of our activities, particularly the daily sampling of HiVol filters over a period of more than one decade. We thank Claudia Zellweger-Faesi, Nicole Bruggisser and David Steger from Empa for supporting the filter collection.

Robin Lewis Modini is thanked for fruitful discussions and Xenia Kipouros is thanked for supporting filter water extraction at PSI.

The authors wish to thank Marie Labat Saint Vincent for punching and transporting PM_{10} samples to Grenoble, and the AirOSol and PANDA analytical platforms at IGE (Institute of Environmental Geosciences, Grenoble, France) for providing laboratory facilities and technical support for the analysis of PM_{10} filters with IC-MS (Patrick Ginot, Rhabira Elazzouzi and Zoia Poloubinski) and ICP-MS (Antoine Boyer) devices.

https://doi.org/10.5194/egusphere-2026-4141
Preprint. Discussion started: 9 November 2026
© Author(s) 2026. CC BY 4.0 License.



Financial support.

This work received funding support from the Swiss National Science Foundation (SNSF, project numbers: 200021_213071 and PZ00P2_202178) and from the Swiss Federal Office for the Environment, with further support from Digitel AG, Camfil GmbH and all the WeMakeIt ScienceBooster crowdfunding supporters.

The continuous online *in-situ* aerosol measurements at the JFJ receive financial support from MeteoSwiss in the framework of the Swiss contribution (GAW-CH) to the Global Atmosphere Watch program of the World Meteorological Organization (WMO), and from the Swiss State Secretariat for Education, Research and Innovation (SERI) in the framework of the Swiss contribution ACTRIS-CH to the ACTRIS ERIC. Measurements conducted by Empa are part of the Swiss National Air Pollution Monitoring Network (NABEL) which is jointly run by Empa and the Swiss Federal Office for the Environment.

The AirOSol and PANDA analytical platforms at IGE were supported by different fundings: the IC-MS and ICP-MS were funded through a donation from Thermo Fisher to the UGA Foundation as part of the Ice Memory program; the LEFE CHAT program with PMOA project (Organic Acids in Atmospheric PM, AO 2022) provided financial support for method validation and part of JFJ PM_{10} analysis.

https://doi.org/10.5194/egusphere-2026-4141
Preprint. Discussion started: 9 November 2026
© Author(s) 2026. CC BY 4.0 License.

References

Algeo, T. J., Wei, W., Remírez, M. N., Wang, C., Liu, Z., Gilleaudeau, G. J., and Brocks, J. J.: Influence of clay-mineral assemblages on the B/Ga salinity proxy, Chemical Geology, 688, 122 837, https://doi.org/10.1016/j.chemgeo.2025.122837, 2025.

Baltensperger, U., Gäggeler, H. W., Jost, D. T., Lugauer, M., Schwikowski, M., Weingartner, E., and Seibert, P.: Aerosol climatology at the high-alpine site Jungfraujoch, Switzerland, Journal of Geophysical Research: Atmospheres, 102, 19 707–19 715, https://doi.org/10.1029/97JD00928, 1997.

Banks, J. R., Hünerbein, A., Heinold, B., Brindley, H. E., Deneke, H., and Schepanski, K.: The sensitivity of the colour of dust in MSG-SEVIRI Desert Dust infrared composite imagery to surface and atmospheric conditions, Atmospheric Chemistry and Physics, 19, 6893–6911, https://doi.org/10.5194/acp-19-6893-2019, 2019.

Bauer, S. E., Mishchenko, M. I., Lacis, A. A., Zhang, S., Perlwitz, J., and Metzger, S. M.: Do sulfate and nitrate coatings on mineral dust have important effects on radiative properties and climate modeling?, Journal of Geophysical Research: Atmospheres, 112, https://doi.org/10.1029/2005JD006977, 2007.

Birch, M. E. and Cary, R. A.: Elemental Carbon-Based Method for Monitoring Occupational Exposures to Particulate Diesel Exhaust, Aerosol Science and Technology, 25, 221–241, https://doi.org/10.1080/02786829608965393, 1996.

Boose, Y., Welti, A., Atkinson, J., Ramelli, F., Danielczok, A., Bingemer, H. G., Plötze, M., Sierau, B., Kanji, Z. A., and Lohmann, U.: Heterogeneous ice nucleation on dust particles sourced from nine deserts worldwide – Part 1: Immersion freezing, Atmospheric Chemistry and Physics, 16, 15 075–15 095, https://doi.org/10.5194/acp-16-15075-2016, 2016.

Boose, Y., Baloh, P., Plötze, M., Ofner, J., Grothe, H., Sierau, B., Lohmann, U., and Kanji, Z. A.: Heterogeneous ice nucleation on dust particles sourced from nine deserts worldwide – Part 2: Deposition nucleation and condensation freezing, Atmospheric Chemistry and Physics, 19, 1059–1076, https://doi.org/10.5194/acp-19-1059-2019, 2019.

Breiter, K., Vašinová Galiová, M., Hložková, M., Korbelová, Z., Kynický, J., and Costi, H. T.: Trace element composition of micas from rare-metal granites of different geochemical affiliations, Lithos, 446-447, 107 135, https://doi.org/10.1016/j.lithos.2023.107135, 2023.

Brunner, C., Brem, B. T., Collaud Coen, M., Conen, F., Hervo, M., Henne, S., Steinbacher, M., Gysel-Beer, M., and Kanji, Z. A.: The contribution of Saharan dust to the ice-nucleating particle concentrations at the High Altitude Station Jungfraujoch (3580 m a.s.l.), Switzerland, Atmospheric Chemistry and Physics, 21, 18 029–18 053, https://doi.org/10.5194/acp-21-18029-2021, 2021.

Bukowiecki, N., Zieger, P., Weingartner, E., Jurányi, Z., Gysel, M., Neininger, B., Schneider, B., Hueglin, C., Ulrich, A., Wichser, A., Henne, S., Brunner, D., Kaegi, R., Schwikowski, M., Tobler, L., Wienhold, F. G., Engel, I., Buchmann, B., Peter, T., and Baltensperger, U.: Ground-based and airborne in-situ measurements of the Eyjafjallajökull volcanic aerosol plume in Switzerland in spring 2010, Atmospheric Chemistry and Physics, 11, 10 011–10 030, https://doi.org/10.5194/acp-11-10011-2011, 2011.

Bukowiecki, N., Weingartner, E., Gysel, M., Coen, M. C., Zieger, P., Herrmann, E., Steinbacher, M., Gäggeler, H. W., and Baltensperger, U.: A Review of More than 20 Years of Aerosol Observation at the High Altitude Research Station Jungfraujoch, Switzerland (3580 m asl), Aerosol and Air Quality Research, 16, 764–788, https://doi.org/10.4209/aaqr.2015.05.0305, 2016.

Cai, W. K., Liu, J. H., Zhou, C. H., Keeling, J., and Glasmacher, U. A.: Structure, genesis and resources efficiency of dolomite: New insights and remaining enigmas, Chemical Geology, 573, 120 191, https://doi.org/10.1016/j.chemgeo.2021.120191, 2021.

Caquineau, S., Gaudichet, A., Gomes, L., Magonthier, M.-C., and Chatenet, B.: Saharan dust: Clay ratio as a relevant tracer to assess the origin of soil-derived aerosols, Geophysical Research Letters, 25, 983–986, https://doi.org/10.1029/98GL00569, 1998.

https://doi.org/10.5194/egusphere-2026-4141
Preprint. Discussion started: 9 November 2026
© Author(s) 2026. CC BY 4.0 License.

Cho, S.-H., Richmond-Bryant, J., Thornburg, J., Portzer, J., Vanderpool, R., Cavender, K., and Rice, J.: A literature review of concentrations and size distributions of ambient airborne Pb-containing particulate matter, Atmospheric Environment, 45, 5005–5015, https://doi.org/10.1016/j.atmosenv.2011.05.009, 2011.

Chou, C., Stetzer, O., Weingartner, E., Jurányi, Z., Kanji, Z. A., and Lohmann, U.: Ice nuclei properties within a Saharan dust event at the Jungfraujoch in the Swiss Alps, Atmospheric Chemistry and Physics, 11, 4725–4738, https://doi.org/10.5194/acp-11-4725-2011, 2011.

Chow, J. C., Watson, J. G., Crow, D., Lowenthal, D. H., and Merrifield, T.: Comparison of IMPROVE and NIOSH Carbon Measurements, Aerosol Science and Technology, 34, 23–34, https://doi.org/10.1080/02786820119073, 2001.

Collaud Coen, M., Weingartner, E., Schaub, D., Hueglin, C., Corrigan, C., Henning, S., Schwikowski, M., and Baltensperger, U.: Saharan dust events at the Jungfraujoch: detection by wavelength dependence of the single scattering albedo and first climatology analysis, Atmospheric Chemistry and Physics, 4, 2465–2480, https://doi.org/10.5194/acp-4-2465-2004, 2004.

Collaud Coen, M., Weingartner, E., Furger, M., Nyeki, S., Prévôt, A. S. H., Steinbacher, M., and Baltensperger, U.: Aerosol climatology and planetary boundary influence at the Jungfraujoch analyzed by synoptic weather types, Atmospheric Chemistry and Physics, 11, 5931–5944, https://doi.org/10.5194/acp-11-5931-2011, 2011.

Collaud Coen, M., Brem, B. T., Gysel-Beer, M., Modini, R., Henne, S., Steinbacher, M., Putero, D., Gini, M. I., and Eleftheriadis, K.: Detection and climatology of Saharan dust frequency and mass at the Jungfraujoch (3580 m a.s.l., Switzerland), Atmospheric Chemistry and Physics, 26, 1623–1645, https://doi.org/10.5194/acp-26-1623-2026, 2026.

Creamean, J. M., Suski, K. J., Rosenfeld, D., Cazorla, A., DeMott, P. J., Sullivan, R. C., White, A. B., Ralph, F. M., Minnis, P., Comstock, J. M., Tomlinson, J. M., and Prather, K. A.: Dust and Biological Aerosols from the Sahara and Asia Influence Precipitation in the Western U.S., Science, 339, 1572–1578, https://doi.org/10.1126/science.1227279, 2013.

Cziczo, D. J., Froyd, K. D., Gallavardin, S. J., Moehler, O., Benz, S., Saathoff, H., and Murphy, D. M.: Deactivation of ice nuclei due to atmospherically relevant surface coatings, Environmental Research Letters, 4, 044 013, https://doi.org/10.1088/1748-9326/4/4/044013, 2009.

Cziczo, D. J., Froyd, K. D., Hoose, C., Jensen, E. J., Diao, M., Zondlo, M. A., Smith, J. B., Twohy, C. H., and Murphy, D. M.: Clarifying the Dominant Sources and Mechanisms of Cirrus Cloud Formation, Science, 340, 1320–1324, https://doi.org/10.1126/science.1234145, 2013.

Di Biagio, C., Formenti, P., Balkanski, Y., Caponi, L., Cazaunau, M., Pangui, E., Journet, E., Nowak, S., Andreae, M. O., Kandler, K., Saeed, T., Piketh, S., Seibert, D., Williams, E., and Doussin, J.-F.: Complex refractive indices and single-scattering albedo of global dust aerosols in the shortwave spectrum and relationship to size and iron content, Atmospheric Chemistry and Physics, 19, 15 503–15 531, https://doi.org/10.5194/acp-19-15503-2019, 2019.

Eggenkamp, H. G. M., Louvat, P., Agrinier, P., Bonifacie, M., Bekker, A., Krupenik, V., Griffioen, J., Horita, J., Brocks, J. J., and Bagheri, R.: The bromine and chlorine isotope composition of primary halite deposits and their significance for the secular isotope composition of seawater, Geochimica et Cosmochimica Acta, 264, 13–29, https://doi.org/10.1016/j.gca.2019.08.005, 2019.

Feinberg, A., Maliki, M., Stenke, A., Sudret, B., Peter, T., and Winkel, L. H. E.: Mapping the drivers of uncertainty in atmospheric selenium deposition with global sensitivity analysis, Atmospheric Chemistry and Physics, 20, 1363–1390, https://doi.org/10.5194/acp-20-1363-2020, 2020.

Fleischer, M.: The abundance and distribution of the chemical elements in the earth's crust, Journal of Chemical Education, 31, 446, https://doi.org/10.1021/ed031p446, 1954.

https://doi.org/10.5194/egusphere-2026-4141
Preprint. Discussion started: 9 November 2026
© Author(s) 2026. CC BY 4.0 License.

Gaston, C. J.: Re-examining Dust Chemical Aging and Its Impacts on Earth's Climate, Accounts of Chemical Research, 53, 1005–1013, https://doi.org/10.1021/acs.accounts.0c00102, 2020.

Gonzalez, R. O., Strekopytov, S., Amato, F., Querol, X., Reche, C., and Weiss, D.: New Insights from Zinc and Copper Isotopic Compositions into the Sources of Atmospheric Particulate Matter from Two Major European Cities, Environmental Science & Technology, 50, 9816–9824, https://doi.org/10.1021/acs.est.6b00863, 2016.

Gonçalves Ageitos, M., Obiso, V., Miller, R. L., Jorba, O., Klose, M., Dawson, M., Balkanski, Y., Perlwitz, J., Basart, S., Di Tomaso, E., Escribano, J., Macchia, F., Montané, G., Mahowald, N. M., Green, R. O., Thompson, D. R., and Pérez García-Pando, C.: Modeling dust mineralogical composition: sensitivity to soil mineralogy atlases and their expected climate impacts, Atmospheric Chemistry and Physics, 23, 8623–8657, https://doi.org/10.5194/acp-23-8623-2023, 2023.

Green, R. O., Mahowald, N., Ung, C., Thompson, D. R., Bator, L., Bennet, M., Bernas, M., Blackway, N., Bradley, C., Cha, J., Clark, P., Clark, R., Cloud, D., Diaz, E., Ben Dor, E., Duren, R., Eastwood, M., Ehlmann, B. L., Fuentes, L., Ginoux, P., Gross, J., He, Y., Kalashnikova, O., Kert, W., Keymeulen, D., Klimesh, M., Ku, D., Kwong-Fu, H., Liggett, E., Li, L., Lundeen, S., Makowski, M. D., Mazer, A., Miller, R., Mouroulis, P., Oaida, B., Okin, G. S., Ortega, A., Oyake, A., Nguyen, H., Pace, T., Painter, T. H., Pempejian, J., Garcia-Pando, C. P., Pham, T., Phillips, B., Pollock, R., Purcell, R., Realmuto, V., Schoolcraft, J., Sen, A., Shin, S., Shaw, L., Soriano, M., Swayze, G., Thingvold, E., Vaid, A., and Zan, J.: The Earth Surface Mineral Dust Source Investigation: An Earth Science Imaging Spectroscopy Mission, in: 2020 IEEE Aerospace Conference, pp. 1–15, ISSN 1095-323X, https://doi.org/10.1109/AERO47225.2020.9172731, 2020.

Gresser, M. J., Tracey, A. S., and Parkinson, K. M.: Vanadium(V) oxyanions: the interaction of vanadate with pyrophosphate, phosphate, and arsenate, Journal of the American Chemical Society, 108, 6229–6234, https://doi.org/10.1021/ja00280a020, 1986.

Gómez Maqueo Anaya, S., Althausen, D., Faust, M., Baars, H., Heinold, B., Hofer, J., Tegen, I., Ansmann, A., Engelmann, R., Skupin, A., Heese, B., and Schepanski, K.: The implementation of dust mineralogy in COSMO5.05-MUSCAT, Geoscientific Model Development, 17, 1271–1295, https://doi.org/10.5194/gmd-17-1271-2024, 2024.

Harr, B., Pu, B., and Jin, Q.: The emission, transport, and impacts of the extreme Saharan dust storm of 2015, Atmospheric Chemistry and Physics, 24, 8625–8651, https://doi.org/10.5194/acp-24-8625-2024, 2024.

Henne, S., Brunner, D., Folini, D., Solberg, S., Klausen, J., and Buchmann, B.: Assessment of parameters describing representativeness of air quality in-situ measurement sites, Atmospheric Chemistry and Physics, 10, 3561–3581, https://doi.org/10.5194/acp-10-3561-2010, 2010.

Herrmann, E., Weingartner, E., Henne, S., Vuilleumier, L., Bukowiecki, N., Steinbacher, M., Conen, F., Collaud Coen, M., Hammer, E., Jurányi, Z., Baltensperger, U., and Gysel, M.: Analysis of long-term aerosol size distribution data from Jungfraujoch with emphasis on free tropospheric conditions, cloud influence, and air mass transport, Journal of Geophysical Research: Atmospheres, 120, 9459–9480, https://doi.org/10.1002/2015JD023660, 2015.

Hooper, J. and Marx, S.: A global doubling of dust emissions during the Anthropocene?, Global and Planetary Change, 169, 70–91, https://doi.org/10.1016/j.gloplacha.2018.07.003, 2018.

Huang, X., Song, Y., Zhao, C., Li, M., Zhu, T., Zhang, Q., and Zhang, X.: Pathways of sulfate enhancement by natural and anthropogenic mineral aerosols in China, Journal of Geophysical Research: Atmospheres, 119, 14,165–14,179, https://doi.org/10.1002/2014JD022301, 2014.

Hueglin, C., Buchmann, B., Steinbacher, M., and Emmenegger, L.: The Swiss National Air Pollution Monitoring Network (NABEL) – Bridging Science and Environmental Policy, CHIMIA, 78, 722–727, https://doi.org/10.2533/chimia.2024.722, 2024.

Inness, A., Ades, M., Agustí-Panareda, A., Barré, J., Benedictow, A., Blechschmidt, A.-M., Dominguez, J. J., Engelen, R., Eskes, H., Flemming, J., Huijnen, V., Jones, L., Kipling, Z., Massart, S., Parrington, M., Peuch, V.-H., Razinger, M., Remy, S., Schulz, M., and Suttie, M.:

https://doi.org/10.5194/egusphere-2026-4141
Preprint. Discussion started: 9 November 2026
© Author(s) 2026. CC BY 4.0 License.

The CAMS reanalysis of atmospheric composition, Atmospheric Chemistry and Physics, 19, 3515–3556, https://doi.org/10.5194/acp-19-3515-2019, 2019.

Jickells, T. D., An, Z. S., Andersen, K. K., Baker, A. R., Bergametti, G., Brooks, N., Cao, J. J., Boyd, P. W., Duce, R. A., Hunter, K. A., Kawahata, H., Kubilay, N., laRoche, J., Liss, P. S., Mahowald, N., Prospero, J. M., Ridgwell, A. J., Tegen, I., and Torres, R.: Global Iron Connections Between Desert Dust, Ocean Biogeochemistry, and Climate, Science, 308, 67–71, https://doi.org/10.1126/science.1105959, 2005.

Johnson, M. S. and Meskhidze, N.: Atmospheric dissolved iron deposition to the global oceans: effects of oxalate-promoted Fe dissolution, photochemical redox cycling, and dust mineralogy, Geoscientific Model Development, 6, 1137–1155, https://doi.org/10.5194/gmd-6-1137-2013, 2013.

Jurányi, Z., Gysel, M., Weingartner, E., DeCarlo, P. F., Kammermann, L., and Baltensperger, U.: Measured and modelled cloud condensation nuclei number concentration at the high alpine site Jungfraujoch, Atmospheric Chemistry and Physics, 10, 7891–7906, https://doi.org/10.5194/acp-10-7891-2010, 2010.

Knippertz, P. and Todd, M. C.: Mineral dust aerosols over the Sahara: Meteorological controls on emission and transport and implications for modeling, Reviews of Geophysics, 50, https://doi.org/10.1029/2011RG000362, 2012.

Kok, J. F., Ridley, D. A., Zhou, Q., Miller, R. L., Zhao, C., Heald, C. L., Ward, D. S., Albani, S., and Haustein, K.: Smaller desert dust cooling effect estimated from analysis of dust size and abundance, Nature Geoscience, 10, 274–278, https://doi.org/10.1038/ngeo2912, 2017.

Kok, J. F., Adebiyi, A. A., Albani, S., Balkanski, Y., Checa-Garcia, R., Chin, M., Colarco, P. R., Hamilton, D. S., Huang, Y., Ito, A., Klose, M., Li, L., Mahowald, N. M., Miller, R. L., Obiso, V., Pérez García-Pando, C., Rocha-Lima, A., and Wan, J. S.: Contribution of the world's main dust source regions to the global cycle of desert dust, Atmospheric Chemistry and Physics, 21, 8169–8193, https://doi.org/10.5194/acp-21-8169-2021, 2021.

Kok, J. F., Storelvmo, T., Karydis, V. A., Adebiyi, A. A., Mahowald, N. M., Evan, A. T., He, C., and Leung, D. M.: Mineral dust aerosol impacts on global climate and climate change, Nature Reviews Earth & Environment, 4, 71–86, https://doi.org/10.1038/s43017-022-00379-5, 2023.

Limmer, D. R., Böning, P., Giosan, L., Ponton, C., Köhler, C. M., Cooper, M. J., Tabrez, A. R., and Clift, P. D.: Geochemical record of Holocene to Recent sedimentation on the Western Indus continental shelf, Arabian Sea, Geochemistry, Geophysics, Geosystems, 13, https://doi.org/10.1029/2011GC003845, 2012a.

Limmer, D. R., Köhler, C. M., Hillier, S., Moreton, S. G., Tabrez, A. R., and Clift, P. D.: Chemical weathering and provenance evolution of Holocene–Recent sediments from the Western Indus Shelf, Northern Arabian Sea inferred from physical and mineralogical properties, Marine Geology, 326-328, 101–115, https://doi.org/10.1016/j.margeo.2012.07.009, 2012b.

Masoom, A., Kazadzis, S., Modini, R. L., Gysel-Beer, M., Gröbner, J., Coen, M. C., Navas-Guzman, F., Kouremeti, N., Brem, B. T., Nowak, N. K., Martucci, G., Hervo, M., and Erb, S.: Long range transport of Canadian Wildfire smoke to Europe in Fall 2023: aerosol properties and spectral features of smoke particles, EGUsphere, pp. 1–43, https://doi.org/10.5194/egusphere-2025-2755, 2025.

Moore, C. M., Mills, M. M., Arrigo, K. R., Berman-Frank, I., Bopp, L., Boyd, P. W., Galbraith, E. D., Geider, R. J., Guieu, C., Jaccard, S. L., Jickells, T. D., La Roche, J., Lenton, T. M., Mahowald, N. M., Marañón, E., Marinov, I., Moore, J. K., Nakatsuka, T., Oschlies, A., Saito, M. A., Thingstad, T. F., Tsuda, A., and Ulloa, O.: Processes and patterns of oceanic nutrient limitation, Nature Geoscience, 6, 701–710, https://doi.org/10.1038/ngeo1765, 2013.

Moteki, N., Adachi, K., Ohata, S., Yoshida, A., Harigaya, T., Koike, M., and Kondo, Y.: Anthropogenic iron oxide aerosols enhance atmospheric heating, Nature Communications, 8, 15 329, https://doi.org/10.1038/ncomms15329, 2017.

https://doi.org/10.5194/egusphere-2026-4141
Preprint. Discussion started: 9 November 2026
© Author(s) 2026. CC BY 4.0 License.



Moustaka, A., Gkikas, A., Logothetis, S.-A., Flemming, J., Rémy, S., Ades, M., Benedetti, A., Tourpali, K., Amiridis, V., and Kazadzis, S.: Two Decades of Aerosol Optical Depth evolution from CAMS Reanalysis, EGUsphere, pp. 1–61, https://doi.org/10.5194/egusphere-2026-1107, 2026.

Möhler, O., Benz, S., Saathoff, H., Schnaiter, M., Wagner, R., Schneider, J., Walter, S., Ebert, V., and Wagner, S.: The effect of organic coating on the heterogeneous ice nucleation efficiency of mineral dust aerosols, Environmental Research Letters, 3, 025 007, https://doi.org/10.1088/1748-9326/3/2/025007, 2008.

Nickovic, S., Vukovic, A., Vujadinovic, M., Djurdjevic, V., and Pejanovic, G.: Technical Note: High-resolution mineralogical database of dust-productive soils for atmospheric dust modeling, Atmospheric Chemistry and Physics, 12, 845–855, https://doi.org/10.5194/acp-12-845-2012, 2012.

Négrel, P., Ladenberger, A., Reimann, C., Birke, M., and Sadeghi, M.: Distribution of Rb, Ga and Cs in agricultural land soils at European continental scale (GEMAS): Implications for weathering conditions and provenance, Chemical Geology, 479, 188–203, https://doi.org/10.1016/j.chemgeo.2018.01.009, 2018.

Park, J., Jang, M., and Yu, Z.: Heterogeneous Photo-oxidation of SO2 in the Presence of Two Different Mineral Dust Particles: Gobi and Arizona Dust, Environmental Science & Technology, 51, 9605–9613, https://doi.org/10.1021/acs.est.7b00588, 2017.

Platnick, S., Hubanks, P., Meyer, K., and King, M.: MODIS Atmosphere L3 Daily Product. NASA MODIS Adaptive Processing System, Goddard Space Flight Center, USA, https://doi.org/10.5067/MODIS/MYD08_D3.061, 2015a.

Platnick, S., Hubanks, P., Meyer, K., and King, M.: MODIS Atmosphere L3 Daily Product. NASA MODIS Adaptive Processing System, Goddard Space Flight Center, USA, https://doi.org/10.5067/MODIS/MOD08_D3.061, 2015b.

Ratcliffe, N. G., Ryder, C. L., Bellouin, N., Woodward, S., Jones, A., Johnson, B., Wieland, L.-M., Dollner, M., Gasteiger, J., and Weinzierl, B.: Long-range transport of coarse mineral dust: an evaluation of the Met Office Unified Model against aircraft observations, Atmospheric Chemistry and Physics, 24, 12 161–12 181, https://doi.org/10.5194/acp-24-12161-2024, 2024.

Rodríguez, S., Alastuey, A., Alonso-Pérez, S., Querol, X., Cuevas, E., Abreu-Afonso, J., Viana, M., Pérez, N., Pandolfi, M., and de la Rosa, J.: Transport of desert dust mixed with North African industrial pollutants in the subtropical Saharan Air Layer, Atmospheric Chemistry and Physics, 11, 6663–6685, https://doi.org/10.5194/acp-11-6663-2011, 2011.

Ryder, C. L., Highwood, E. J., Walser, A., Seibert, P., Philipp, A., and Weinzierl, B.: Coarse and giant particles are ubiquitous in Saharan dust export regions and are radiatively significant over the Sahara, Atmospheric Chemistry and Physics, 19, 15 353–15 376, https://doi.org/10.5194/acp-19-15353-2019, 2019.

Sayer, A. M., Hsu, N. C., Lee, J., Kim, W. V., and Dutcher, S. T.: Validation, Stability, and Consistency of MODIS Collection 6.1 and VIIRS Version 1 Deep Blue Aerosol Data Over Land, Journal of Geophysical Research: Atmospheres, 124, 4658–4688, https://doi.org/10.1029/2018JD029598, 2019.

Schepanski, K., Tegen, I., Laurent, B., Heinold, B., and Macke, A.: A new Saharan dust source activation frequency map derived from MSG-SEVIRI IR-channels, Geophysical Research Letters, 34, https://doi.org/10.1029/2007GL030168, 2007.

Schepanski, K., Tegen, I., and Macke, A.: Comparison of satellite based observations of Saharan dust source areas, Remote Sensing of Environment, 123, 90–97, https://doi.org/10.1016/j.rse.2012.03.019, 2012.

Scheuvens, D., Schütz, L., Kandler, K., Ebert, M., and Weinbruch, S.: Bulk composition of northern African dust and its source sediments — A compilation, Earth-Science Reviews, 116, 170–194, https://doi.org/10.1016/j.earscirev.2012.08.005, 2013.

https://doi.org/10.5194/egusphere-2026-4141
Preprint. Discussion started: 9 November 2026
© Author(s) 2026. CC BY 4.0 License.

Schmetz, J., Pili, P., Tjemkes, S., Just, D., Kerkmann, J., Rota, S., and Ratier, A.: AN INTRODUCTION TO METEOSAT SECOND GENERATION (MSG), Bulletin of the American Meteorological Society, 83, 977–992, https://doi.org/10.1175/1520-0477(2002)083<0977:AITMSG>2.3.CO;2, 2002.

Schulz, M., Prospero, J. M., Baker, A. R., Dentener, F., Ickes, L., Liss, P. S., Mahowald, N. M., Nickovic, S., García-Pando, C. P., Rodríguez, S., Sarin, M., Tegen, I., and Duce, R. A.: Atmospheric Transport and Deposition of Mineral Dust to the Ocean: Implications for Research Needs, Environmental Science & Technology, 46, 10 390–10 404, https://doi.org/10.1021/es300073u, 2012.

Schwikowski, M., Seibert, P., Baltensperger, U., and Gaggeler, H. W.: A study of an outstanding Saharan dust event at the high-alpine site Jungfraujoch, Switzerland, Atmospheric Environment, 29, 1829–1842, https://doi.org/10.1016/1352-2310(95)00060-C, 1995.

Seinfeld, J. H., Carmichael, G. R., Arimoto, R., Conant, W. C., Brechtel, F. J., Bates, T. S., Cahill, T. A., Clarke, A. D., Doherty, S. J., Flatau, P. J., Huebert, B. J., Kim, J., Markowicz, K. M., Quinn, P. K., Russell, L. M., Russell, P. B., Shimizu, A., Shinozuka, Y., Song, C. H., Tang, Y., Uno, I., Vogelmann, A. M., Weber, R. J., Woo, J.-H., and Zhang, X. Y.: ACE-ASIA: Regional Climatic and Atmospheric Chemical Effects of Asian Dust and Pollution, Bulletin of the American Meteorological Society, 85, 367–380, https://doi.org/10.1175/BAMS-85-3-367, 2004.

Shafer, M. M., Toner, B. M., Overdier, J. T., Schauer, J. J., Fakra, S. C., Hu, S., Herner, J. D., and Ayala, A.: Chemical Speciation of Vanadium in Particulate Matter Emitted from Diesel Vehicles and Urban Atmospheric Aerosols, Environmental Science & Technology, 46, 189–195, https://doi.org/10.1021/es200463c, 2012.

Sokolik, I. N. and Toon, O. B.: Incorporation of mineralogical composition into models of the radiative properties of mineral aerosol from UV to IR wavelengths, Journal of Geophysical Research: Atmospheres, 104, 9423–9444, https://doi.org/10.1029/1998JD200048, 1999.

Song, Q., Ginoux, P., Gonçalves Ageitos, M., Miller, R. L., Obiso, V., and Pérez García-Pando, C.: Modeling impacts of dust mineralogy on fast climate response, Atmospheric Chemistry and Physics, 24, 7421–7446, https://doi.org/10.5194/acp-24-7421-2024, 2024.

Soussé Villa, R., Jorba, O., Gonçalves Ageitos, M., Bowdalo, D., Guevara, M., and Pérez García-Pando, C.: A comprehensive global modeling assessment of nitrate heterogeneous formation on desert dust, Atmospheric Chemistry and Physics, 25, 4719–4753, https://doi.org/10.5194/acp-25-4719-2025, 2025.

Strawn, D. G.: Review of interactions between phosphorus and arsenic in soils from four case studies, Geochemical Transactions, 19, 10, https://doi.org/10.1186/s12932-018-0055-6, 2018.

Sullivan, R. C., Moore, M. J. K., Petters, M. D., Kreidenweis, S. M., Roberts, G. C., and Prather, K. A.: Effect of chemical mixing state on the hygroscopicity and cloud nucleation properties of calcium mineral dust particles, Atmospheric Chemistry and Physics, 9, 3303–3316, https://doi.org/10.5194/acp-9-3303-2009, 2009.

Swap, R., Garstang, M., Greco, S., Talbot, R., and Kållberg, P.: Saharan dust in the Amazon Basin, Tellus B, 44, 133–149, https://doi.org/10.1034/j.1600-0889.1992.t01-1-00005.x, 1992.

Tang, M., Huang, X., Lu, K., Ge, M., Li, Y., Cheng, P., Zhu, T., Ding, A., Zhang, Y., Gligorovski, S., Song, W., Ding, X., Bi, X., and Wang, X.: Heterogeneous reactions of mineral dust aerosol: implications for tropospheric oxidation capacity, Atmospheric Chemistry and Physics, 17, 11 727–11 777, https://doi.org/10.5194/acp-17-11727-2017, 2017.

Tobo, Y., DeMott, P. J., Raddatz, M., Niedermeier, D., Hartmann, S., Kreidenweis, S. M., Stratmann, F., and Wex, H.: Impacts of chemical reactivity on ice nucleation of kaolinite particles: A case study of levoglucosan and sulfuric acid, Geophysical Research Letters, 39, https://doi.org/10.1029/2012GL053007, 2012.

https://doi.org/10.5194/egusphere-2026-4141
Preprint. Discussion started: 9 November 2026
© Author(s) 2026. CC BY 4.0 License.

UNCCD: United Nations Convention to Combat Desertificatio: Sand and dust storms compendium: Information and guidance on assessing and addressing the risks, Tech. rep., Bonn, Germany., https://www.unccd.int/resources/publications/sand-and-dust-storms-compendium-information-and-guidance-assessing-and, 2022.

Uno, K., Okumura, M., Nakao, A., Yamaguchi, A., and Yanai, J.: Cesium stability on the interlayers of K- or Rb-fixing micaceous minerals investigated by both experimental and numerical simulation methods, Science of The Total Environment, 949, 175 012, https://doi.org/10.1016/j.scitotenv.2024.175012, 2024.

Usher, C. R., Michel, A. E., and Grassian, V. H.: Reactions on Mineral Dust, Chemical Reviews, 103, 4883–4940, https://doi.org/10.1021/cr020657y, 2003.

van der Does, M., Korte, L. F., Munday, C. I., Brummer, G.-J. A., and Stuut, J.-B. W.: Particle size traces modern Saharan dust transport and deposition across the equatorial North Atlantic, Atmospheric Chemistry and Physics, 16, 13 697–13 710, https://doi.org/10.5194/acp-16-13697-2016, 2016.

Vlasenko, A., Sjogren, S., Weingartner, E., Stemmler, K., Gäggeler, H. W., and Ammann, M.: Effect of humidity on nitric acid uptake to mineral dust aerosol particles, Atmospheric Chemistry and Physics, 6, 2147–2160, https://doi.org/10.5194/acp-6-2147-2006, 2006.

Warren, J. K.: Depositional Chemistry and Hydrology, in: Evaporites: A Geological Compendium, edited by Warren, J. K., pp. 85–205, Springer International Publishing, Cham, ISBN 978-3-319-13512-0, https://doi.org/10.1007/978-3-319-13512-0_2, 2016a.

Warren, J. K.: Interpreting Evaporite Textures, in: Evaporites: A Geological Compendium, edited by Warren, J. K., pp. 1–83, Springer International Publishing, Cham, ISBN 978-3-319-13512-0, https://doi.org/10.1007/978-3-319-13512-0_1, 2016b.

Weng, J., Hao, Y., Brem, B. T., Cui, T., Khare, P., Dada, L., Daellenbach, K. R., Darfeuil, S., Uzu, G., Jaffrezo, J.-L., Steinbacher, M., Reimann, S., Gkraikou, T., Oikonomou, K., Sciare, J., Collaud Coen, M., Mohr, C., Prévôt, A. S. H., Gysel-Beer, M., El Haddad, I., and Winiger, P.: A Decadal-Scale Perspective on PM10 Composition and its Variability Drivers at the Alpine High-Altitude Research Station Jungfraujoch, EGUsphere, pp. 1–31, https://doi.org/10.5194/egusphere-2026-3660, 2026.

Yu, H., Tan, Q., Zhou, L., Zhou, Y., Bian, H., Chin, M., Ryder, C. L., Levy, R. C., Pradhan, Y., Shi, Y., Song, Q., Zhang, Z., Colarco, P. R., Kim, D., Remer, L. A., Yuan, T., Mayol-Bracero, O., and Holben, B. N.: Observation and modeling of the historic "Godzilla" African dust intrusion into the Caribbean Basin and the southern US in June 2020, Atmospheric Chemistry and Physics, 21, 12 359–12 383, https://doi.org/10.5194/acp-21-12359-2021, 2021.